NASA TECHNICAL MEMORANDUM NASA TM-77509

ON THE FLOW PROCESSES IN SHARPLY INCLINED AND STALLED AIRFOILS IN PARALLEL MOVEMENT AND ROTATION

M. Kohler

(NASA-TM-77509) ON THE FLOW PROCESSES IN SHARPLY INCLINED AND STALLED AIRFOILS IN PARALLEL MOVEMENT AND ROTATION (National Aeronautics and Space Administration) 44 p HC A03/MF A01 CSCL 01A G3/02

N85-16952

Unclas 14141

Translation of "Uber die Strömungsvorgange an steil angestellten und überzogenen Tragflügeln bei Parallelbewegung und Drehung," Luftfahrtforschung, Vol. 16, No. 4, 1939, pp. 158-177.

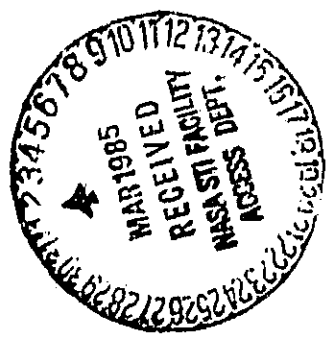

NATIONAL AERONAUCTICS AND SPACE ADMINISTRATION
WASHINGTON, D.C. 20546 SEPTEMBER 1984

STANDARD TITLE PAGE

1. Report No. NASA TM-77509	2. Government Accession No.	3. Recipient's Catalog No.
4. Title and Subtitle ON THE FLOW PROCESSES IN SHARPLY INCLINED AND STALLED AIRFOILS IN PARALLEL MOVEMENT AND ROTATION		5. Report Date September 1984 6. Performing Organization Code
7. Author(s) M. Kohler		8. Performing Organization Report No. 10. Work Unit No.
9. Performing Organization Name and Address Leo Kanner Associates Redwood City, CA 94063		11. Contract or Grant No. NASw 3541 13. Type of Report and Period Covered Translation
12. Sponsoring Agency Name and Address National Aeronautics and Space Administration, Washington, D.C. 20546		14. Sponsoring Agency Code

15. Supplementary Notes Translation of "Uber die Stromungsvorgange an steil angestellten und überzogenen Tragflügeln bei Parallelbewegung und Drehung," Luftfahrtforschung, Vol. 16, No. 4, 1939, pp. 158-177.

16. Abstract

The purpose of this study is to obtain a deeper insight into the complicated flow processes on airfoils in the region of the buoyancy maxima. To this end calculated and experimental investigations are carried out on a straight stationary, a twisted stationary and a straight rotating rectangular wing. According to the available results the method gives results which can be applied sufficiently for flow applied firmly on all sides for all rotation values. The reliability of the method may be questioned for a flow undergoing transition from the attached to the separated state or for totally separated flow and higher rotation values.

17. Key Words (Selected by Author(s))	18. Distribution Statement Unlimited-Unclassified

19. Security Classif. (of this report)	20. Security Classif. (of this page)	21. No. of Pages	22.
Unclassified	Unclassified	44	

ON THE FLOW PROCESSES IN SHARPLY INCLINED AND STALLED AIRFOILS IN PARALLEL MOVEMENT AND ROTATION[1]

M. Kohler, Friedrichshafen/Bodensee

A report of the Aerodynamic Experimental Facility of Göttingen E.V. in the Kaiser Wilhelm Association for the Promotion of Science

/158*

The purpose of this study is to obtain a deeper insight into the complicated flow processes on airfoils in the region of the buoyancy maxima. To this end calculations and experimental investigations are carried out on a straight stationary, a twisted stationary and a straight rotating rectangular wing.

Contents

[1]This study was approved as a thesis by the Faculty of Mechanical Engineering of the Hanover Technical University. D 89.

*Numbers in the margin indicate pagination in the foreign text.

1. Introduction

We know that the nature of the flow on an airfoil changes greatly when the buoyancy maximum is exceeded. The flow starts to become "unsteady" on the top of the wing and is detached from the wing with the further increase of the angle of attack. Detachment can begin locally and then progress over the entire top of the wing. Under certain conditions, however, a sudden separation along the span is also possible. The generally existing formed symmetry of the wing assembly makes one expect a symmetrical course of the processes. This does apply, but in most cases only for a short time, because we are dealing here with weakly stable or labile states of equilibrium. Even a slight disturbance, say by a squall, may cause an asymmetry of the flow along the span and thus cause a dangerous change of the flight position. The stalling aircraft tilts over one end of the wing, gets into a strongly accelerated rotary movement and only reaches a new state of equilibirum in the stationary spin flight.

An attempt is made already when designing the wing assembly to prevent these undesirable flight movements by choosing a suitable buoyancy distribution. The theory of the finite airfoil makes it possible today to give methods of calculation making it possible to obtain such distributions for most modern wing shapes. It assumes that the buoyancy and angle of attack depend mutually in a simple way, and that the resistance against buoyancy remains small. As long as the flow is firmly applied to the wing, these assumptions seem to be fulfilled even for fairly high buoyancy coefficients. But if it begins to be detached, the assumptions no longer apply. Thus the airfoil theory in its present form is no longer valid. It now appears as though the high buoyancy research should be studied more deeply through the boundary layer theory. But this theory too is not yet able to provide

quantitatively applicable methods for understanding these complicated states. The difficulties are increased because in the region of the buoyancy maximum, regions of applied and separated flow occur next to each other, and so far nothing certain may be stated about their interactions, and finally also because in the rotating wing assembly we have to take into account the forces of inertia because of the transition from the reference system at rest to the rotating reference system.

In view of this situation, it seemed to be proper to carry out observations of the flow and measurements of the pressure on sharply inclined and "stalled" airfoils and establish in this connection how far theory agrees with reality. To create clear conditions, airfoil models with rectangular ground plan were used. Of two wings, one was studied stationary, the other rotating in the wind flow. To the measurement results obtained by this means, those of another rectangular wing were added, which was twisted along the span according to a certain degree of rotation.[1]

2. Objects of the Experiments

These three airfoils are grouped and designated as follows for the following sections:

1. Airfoil 1, straight rectangular wing for the experiments without rotation;

2. Airfoil 2, twisted rectangular wing, Fig. 1;

3. Airfoil 3, straight rectangular wing for the experiment under rotation.

---

[1] These measurements were carried out on the suggestion of Professor Dr. Betz, Göttingen, and specifically before the measurement on stationary and rotating airfoils.

The airfoil cross section used was the Göttingen profile 420,[2] which has already been used several times for wind tunnel tests.[3] The models had a span of b = 800 mm and a depth i = 160 mm, that is an aspect ratio i:b=1:5. The model edges were sharp. The measurements were carried out in wind tunnel IV of the aerodynamic experimental facilities of Göttingen, whose normal nozzle has a diameter d=1.50 m and whose "turbulence level" may be indicated as $Re \approx 0.24 \cdot 10^6$ (that is the Re number for the sphere for $c_w=0.3$).[4] The velocity in the blower stream had to be limited with regard to the strength of the rotating model, to be $v_0 \approx 20$ m/s. The Reynolds number of the experiment was accordingly $Re \approx 0.22 \cdot 10^6$ (referred to the wing depth). This basically low Re number plays only a subordinate role within the framework of the comparisons to be carried out here, since all measurement results were obtained under the same conditions.

/159

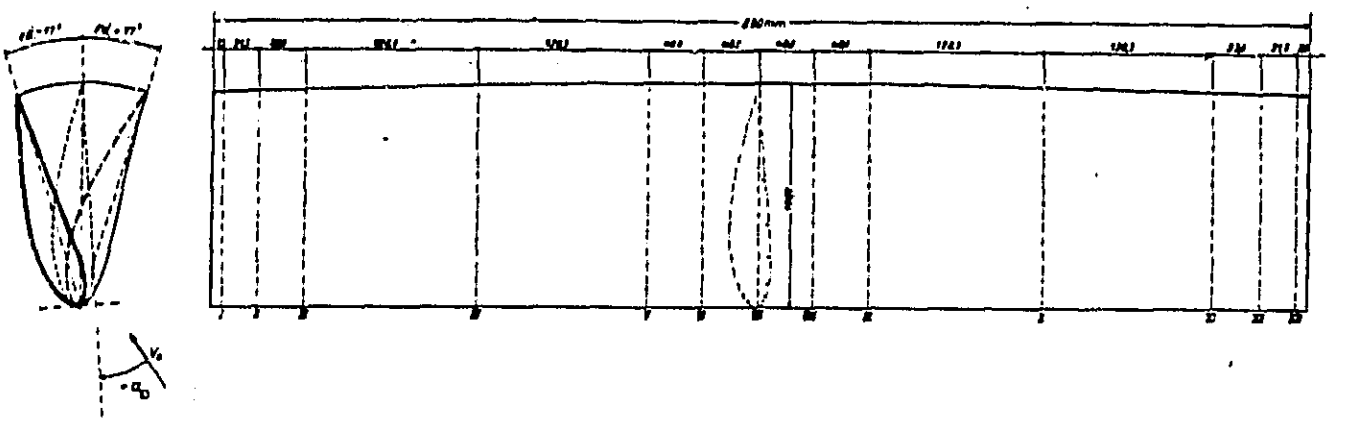

Fig. 1. Sketch of the twisted airfoil 2.

[2] For admeasurements see AVA-Lieferung III, p. 29.

[3] a) Polar measurement: AVA-Lieferung I, p. 108; AVA-Lieferung III, p. 78.
b) Self rotation measurement: O. Schrenk, Z. Flugtechn. Bd. 19, (1929), p. 533.

[4] AVA-Lieferung IV, p. 106, article by O. Flachsbart.

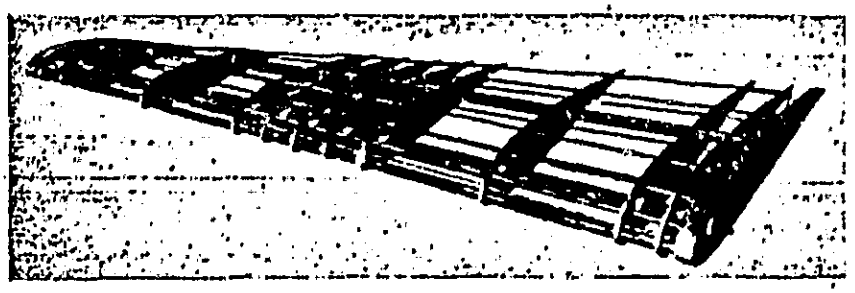

Fig. 2. Metal framework of the twisted airfoil 2.

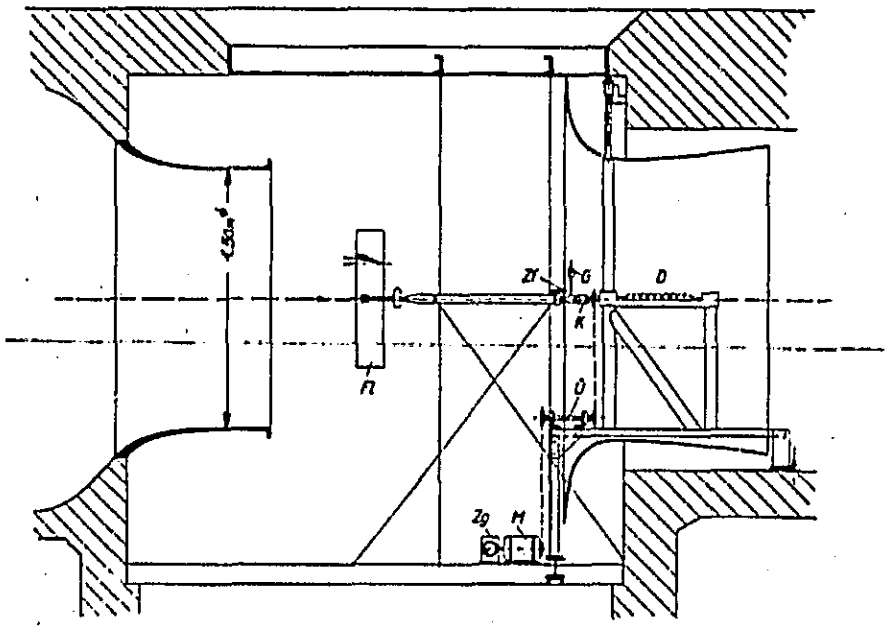

Fig. 3. Scheme of the experimental layout in the wind tunnel. Reduction about 1:30.

D -Pressure transmission instrument; Fl - Airfoil;
G - Compensation weight; K - Elastic coupling;
M - Drive engine; U - Transmission elements;
Zf, Zg - Fine or rough gauge of the speed of revolution

3. Production of the Model

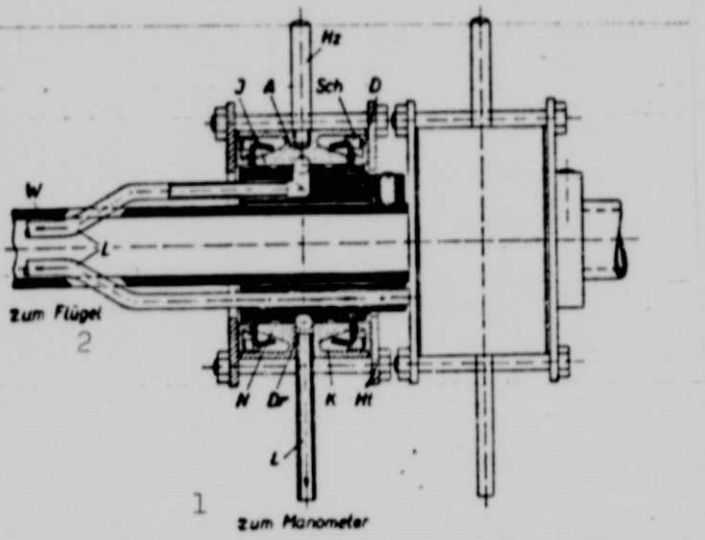

Fig. 4. Pressure transmission equipment. Reduction about 1:1.5.
A - External ring; D - Lid; Dr - Pressurized channel; Hz - Holding journal; Ht - Other holding element; J - Internal ring; K - Sealing chamber; L - Pressurized lines; N - Sealing groove; Sch - Ejection ring; W - Model shaft.

Key: 1. To the manometer; 2. To the wing

Airfoils 1 and 2 were built according to the design commonly used in Göttingen. They consisted of a metal framework which was filled out with gypsum. The carriers of pressure borings were metal ribs, the pressurized lines metal tubes, which were laid out inside the model, Fig. 2.

But a different method of production had to be sought for the airfoil 3, since according to earlier experience, bursting of the gypsum had to be expected at high speeds of rotation. After some preliminary experiments the author decided on a wing in the shape of a full shell. The top and bottom of the airfoil were designed as partial shell in 2 mm thick brass plates, laid out on the inside with pressure pipe lines, and soldered along the seams. Before assembly of the partial shells, a reinforcement element was introduced to it in the center of the wing, which allows the attachment of the wings on the experimental device. The production of the wing required a high degree of craftsmanship.[5]

[5]It was done by Master J. Lotze of KWI Göttingen, whom I would like to thank.

4. Experimental Facilities and Measurement Procedure

Airfoils 1 and 2 were incorporated with the wire suspension commonly used for fixed component measurement in the wind tunnel. This suspension is characterized by the fact that the flow reaches the model without disturbance. Airfoil 3 was attached to the experimental device shown in Fig. 3. This was a rotating device, as is used for self-rotation investigations. It was supplemented for the present experiments by an electrical drive, which allowed the adjustment of certain values of rotation.

The pressure measurement equipment used was a multiple manometer designed by O. Schrenk and the author.[6] The connections between the manometer tubes and the tubes in the airfoil were produced with rubber hoses. The measurement of pressures on airfoils 1 and 2 were carried out by the ordinary method. The /160
pressure distribution for a wing cross section was obtained each time with a single measurement. The pressure borings of the other cross sections were sealed here with a sealing compound. The pressure measurement on the rotating airfoil 3 was organized in a more difficult manner. To transmit the pressures from the rotating system to the manometer at rest in the hole, the "hydraulic connection" shown in Fig. 4 was used. This was an instrument developed by G. Fuhrmann and modified by O. Flachsbart,[7] on which several further changes were made. These changes consisted in the fact that the ejection ring Sch had been given a conical extension and the external ring A a conical twist adjusted to it. This created an additional sealing area, which increased the safety in pressure transmission.

---

[6] Literature: Instruments of AVA-Göttingen; Issue: Micromanometers.

[7] Handbuch der Experimentalphysik (Handbook of Experimental Physics), Vol. 4, Part 3, Article by O. Flachsbart, Propellers, p. 385.

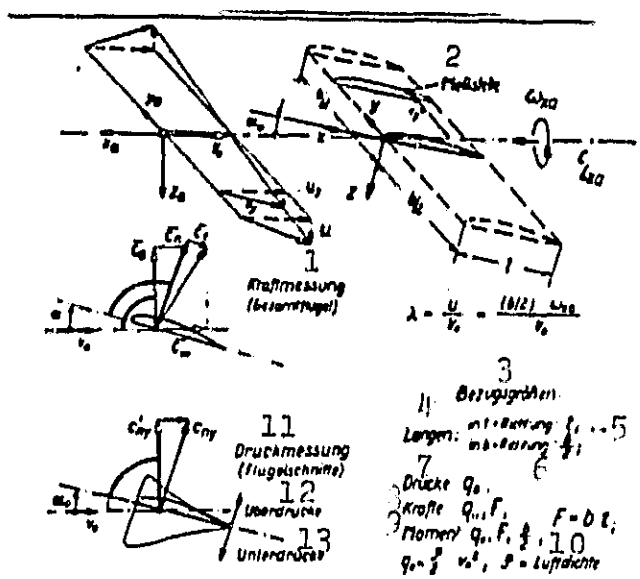

Fig. 5. General definition sketch.

Key: 1. Measurement of power (total wing); 2. Measurement point; 3. Reference quantities; 4. Length; 5. In t direction; 6. In b direction; 7. Pressure: 8. Forces; 9. Momentum; 10. Air density; 11. Pressure measurments (wing cross section); 12. Excess pressures; 13. Under pressures.

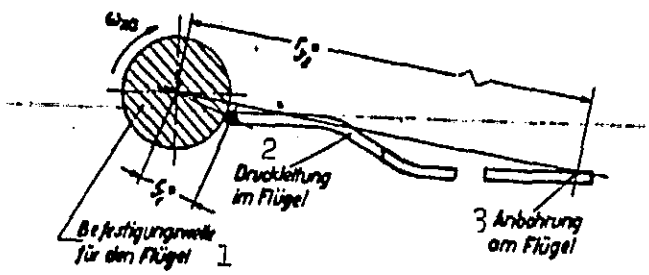

Fig. 6. Definition sketch to take into account the centrifuge pressures of the air masses rotating in the pressure lines.

Key: 1. Attachment shaft for the wing; 2. Pressure line in the wing; 3. Boring in the wing

Nevertheless, the measurement of the pressure was carried out with greatest care.[8] At the beginning of the experiment five connections and later nine such connections were available. Therefore it was impossible to avoid determining the pressure distribution of a wing cross section in several partial measurements. To be able to arrange consecutively the individual results in a proper way, each time one point of the previous partial measurement was measured once again as a control point. But it was found that the velocity in the blower stream and the speed of rotation of the model could be adjusted again with sufficient

[8] In the measurements I was assisted by engineers H. Hennecke and F. Redicker, and in the evaluation by engineer H. Boenecke, whom I would like to thank.

precision after some practice and could be kept uniform, so that a straightening was required only in some cases.

For the pressures measured in the rotating system, a special correction had to be introduced, by which the effect of inertia of the rotating air masses and the pressure lines were taken into consideration.

$$p = p' + p_y^*$$

p = final pressure at the measurement point;

p' = pressure indicated for this measurement point on the manometer;

p_y^* = centrifuge pressure of the air mass enclosed in the measurement line

$$p_y^* = \varrho\,\omega_{xa}^2 \int_{y^* = r_{y1}^*}^{y^* = r_{y2}^*} y^*\,dy^* = \frac{\varrho}{2}\,\omega_{xa}^2 \cdot (r_{y2}^{*2} - r_{y1}^{*2}).$$

For the evaluation we assumed that $r_{y2}^* >> r_{y1}^*$ and r_{y2}^* was written as r_y^*

$$p_y^* = \frac{\varrho}{2}\,(r_y^*\,\omega_{xa})^2 = q_u v^*.$$

that is the centrifuge pressure is equal to the dynamic pressure of the peripheral speed of the measurement point. The asterisk means that we are dealing here with the distance of a point of the system fixed with regard to the airfoil x, y, z (measurement point) from the longitudinal axis x_a (axis of rotation) of the system fixed with regard to the flow x_a, y_a, z_a (see also Figs. 5, 6). The accessory device shown in Fig. 7 was used to obtain r_y^*. /161

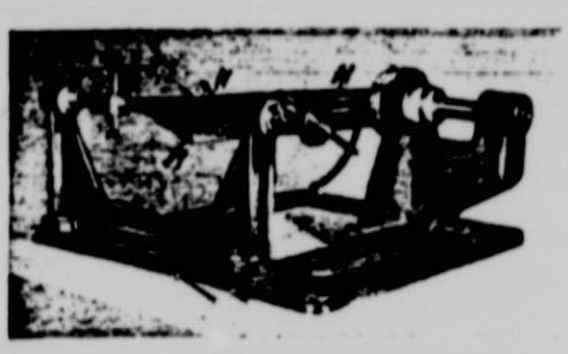

Fig. 7. Accessory device to obtain the distance from the pressure borings on the airfoil 3 from the axis of rotation of the model .

Fl - Airfoil
M - Scale
N - Scanning needle

5. Representation of the Measurement Results

All the pressures p measured and corrected on the airfoils are rendered dimensionless by division by the dynamic pressure q_0 of the undisturbed velocity in the blower stream v_0. Thus we obtained for the sections of the rotating airfoil outside the axis of rotation 3 pressure values, which are more than 1; for the dynamic pressure q_y of the local velocity in the blower stream v_y determining the amount of pressure is greater than q_0 as a result of the local peripheral speed u_y. In the comparison of the measurement results of the twisted airfoil 2 and the rotating airfoil 3, account must be taken of this fact. This was done by multiplying the values of the twisted airfoil by the ratio q_y/q_0.

The dimensionless pressures p/q_0 were plotted for each wing section on the wing chord over the dimensionless distance x/t of the measurement point from the frontmost point of the profile. To improve the clarity of the basically extensive experimental material, each time the pressure distribution pictures of the top and bottom of the wings were put together. The place of separation was the frontmost measurement point, behind the profile tip.[9] Moreover the sum values of these pressure distribution curves

[9] In the first examination of the pressure distribution pictures of the top of the wing it is recommended to turn them by 180°. The pressure curves thus appear somewhat clearer.

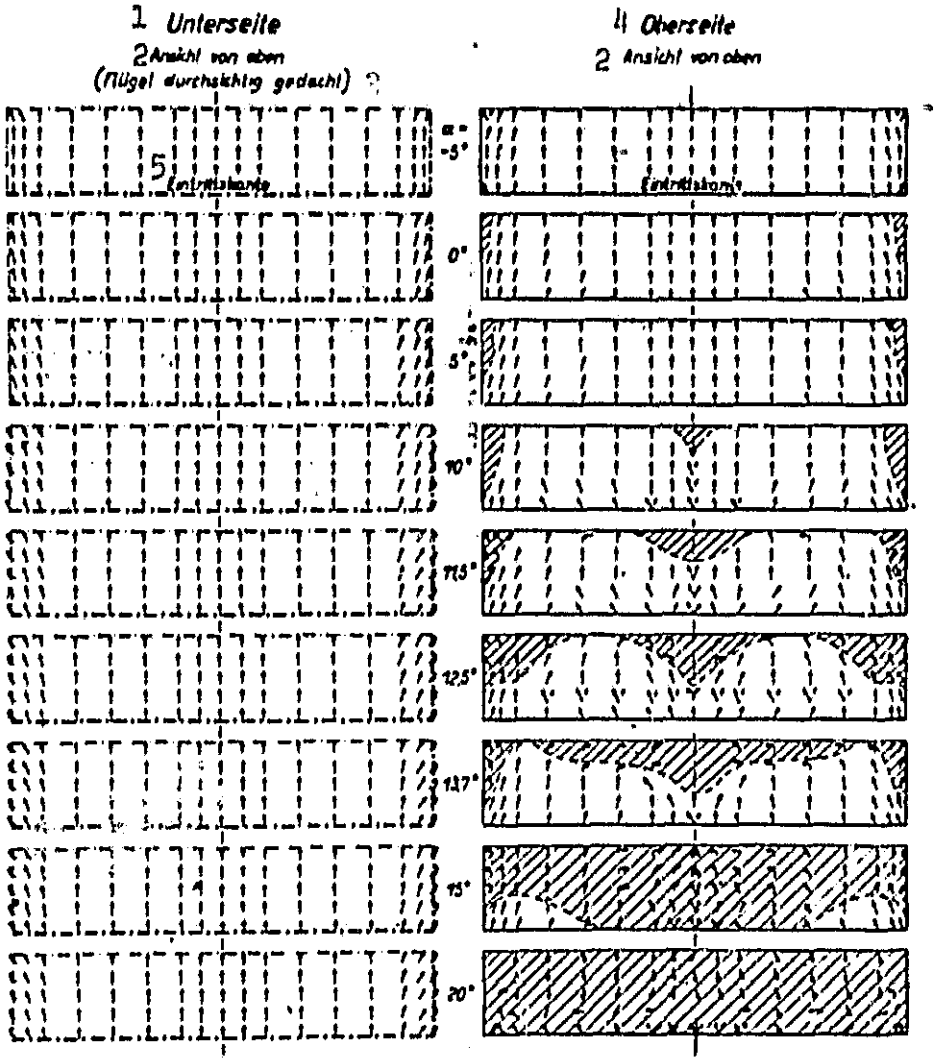

Fig. 8. Fiber probe observation about 1 mm over the surface of the stationary airfoil 1 for different angles of attack.

Key: 1. Bottom; 2. View from the top; 3.(Wing considered transparent); 4. Top; 5. Entrance sides

were represented as local normal force coefficient c_{ny} over the dimensionless distance 2y/b of the measurement section from the center of the wing. Thus it was possible to obtain in the first place by integration along the span the average normal force

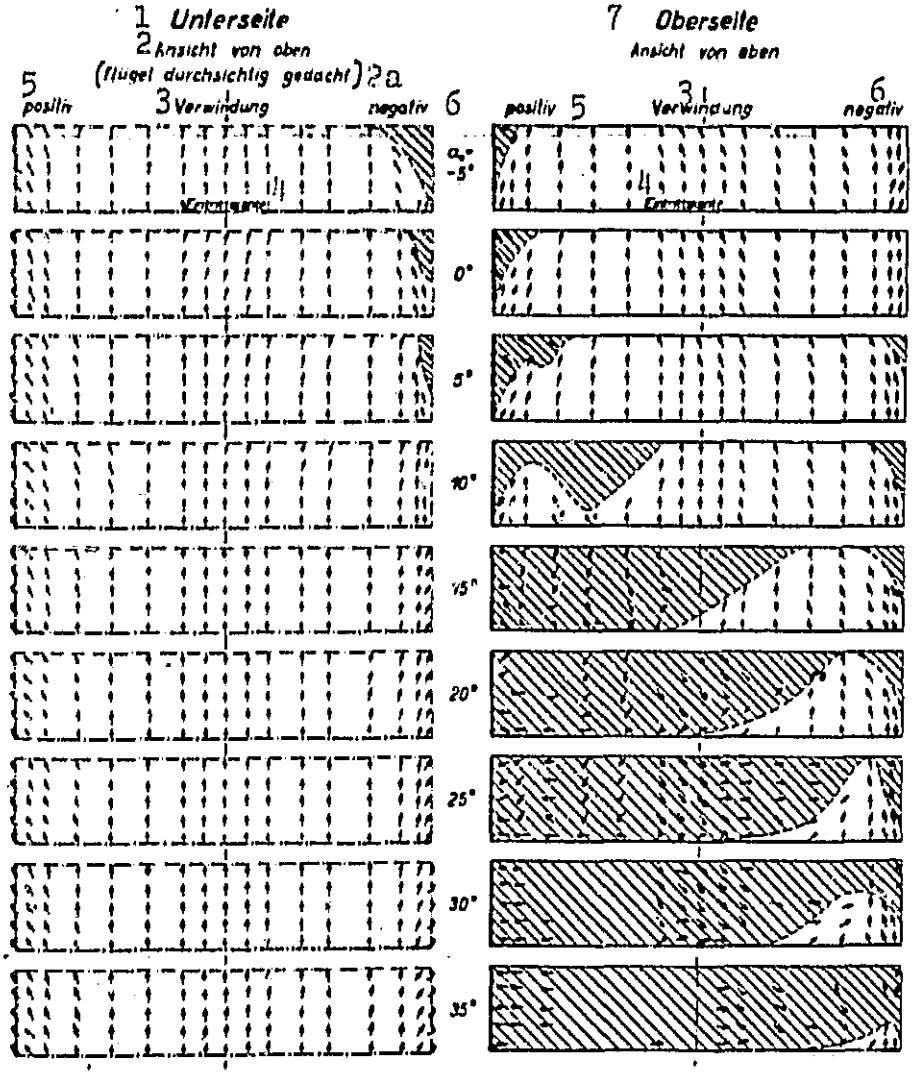

Fig. 9. Fiber probe observations about 1 mm above the surface of the twisted airfoil 2, for different angles of attack.

Key: 1. Bottom; 2. View from the top; 2a. (Wing considered transparent); 3. Twists; 4. Entrance side; 5. Positive; 6. Negative; 7. Top

coefficient $\bar{c}_n$ of airfoils 1 and 3 (for $\lambda=0$) and in the second place to determine through the component c_{ny}' (see Fig. 5) and by introducing the lever arm, the coefficinet c_{Lxa} of the momentum around the axis of rotation of the wing.

6. Range of Measurements and Evaluation

The range of the measurements was as follows:

1. Airfoil 1, straight rectangular wing, $\lambda=0$.

p/q_0, c_{ny} and $\overline{c_n}$ for $\alpha=0$; 5; 10; 15; 20 and 30°.[10] In Fig. 14, moreover, the values of $\overline{c_n}$ are given for $\alpha=35$; 40; 45; 50°. The reproduction of pressure distributions for these angles was omitted, since they are basically similar to the distributions for $\alpha=30°$.

2. Airfoil 2, twisted rectangular wing. Twists along the range according to $\lambda=0.3$.

p/q_0, c_{ny} and c_{Lxa} for $\alpha_0=0$; 5; 10; 15; 20 and 30°.

3. Airfoil 3, straight rectangular wing for $\lambda=0$ or $\lambda\neq0$.

p/q_0, c_{ny} and $\overline{c_n}$ for $\alpha_0=15$; 20 and 30° for $\lambda=0$.

p/q_0, c_{ny} and c_{mLxa} for $\alpha_0=15°$ for $\lambda=0.1$; 0.2 and 0.4; also for $\alpha_0=20$ and 30° for $\lambda=0.1$; 0.2; 0.6 and 0.7.

Moreover fiber probe observations were carried out on the airfoil for several angles of attack and established in the form of sketches, Fig. 8, 9.

The evaluation of the tests extended to: /162

a) a comparison of the theoretical buoyancy distribution with experimental normal force distribution along the span for all three airfoils, insofar as it is at all possible at present;

---

[10] The measurement results were given for the angles of attack α adjusted in the wind tunnel (straight wing 1) and α_0 (central section of the twisted wing 2 and rotating wing 3), to facilitate the classification. The corrections as a result of the finite jet diameter are here:

$\alpha°$ and $\alpha_0°$	0	5	10
$\Delta\alpha°$	−0,2	−0,5	−0,7
$\alpha°$ and $\alpha_0°$	15	(20)	(30)
$\Delta\alpha°$	−0,7	(−0,6)	(−0,5)

b) a comparison of pressure distribution over the center section of the straight airfoil 1 and the twisted airfoil 2;

c) a comparison of the pressure distribution of a section lying comparatively far from the axis of rotation on the left and right hand halves of the airfoil (left and right from the imaginary aircraft pilot) on the rotating and suitably twisted airfoil, and finally;

d) obtaining the range of self-rotation of the studied rectangular wing by means of the curves $c_{mLax}=f(\alpha_0)$ and the comparison with the earlier self rotation measurement on an airfoil of the same profile.[11]

To obtain the theoretical buoyancy distribution the method of calculation of H. Multhopp[12] was taken, which like all methods of this type comes from the Prandtl airfoil theory, it has practically the important advantage that the results can be obtained with considerable saving of time.

The type of assignment of the theoretical and experimental results is discussed in the following remarks.

7. On the Effects of Sationary and Rotating Airfoils

Before discussing the measurement results, it would be proper to study in greater detail the individual effects on stationary and rotating airfoils. The following act:

1. On the stationary airfoil

a) Pressure gradient forces on all particles of the airfoil flow,

b) friction forces of the wall on the particles of the

[11] See footnote 3b.

[12] H. Multhopp, Luftf.-Forschg. Bd. 15 (1938), P. 153.

flow nearest the wall;

c) drag forces from the unseparated external flow on the particles of the friction layer, and specifically in the direction of depth and range; moreover

2. On the rotating airfoil, besides these forces, forces of inertia as a result of

a) the centrifugal acceleration of particles near the wall,

b) the coriolis acceleration of all particles of the airfoil flow, in particular those not belonging to the friction layer.

The effect in the buoyancy region considered here are approximately as follows:

In the direction of depth: on the top; up to the pressure minimum, acceleration of the flow particles, then delay as a result of the increase of pressure; deceleration of the particles nearest the wall with the subsiding drag effect of the external flow; thickening of the friction layer and finally detachment of the flow, generally progressing from the rear forward. In the separated region no more clear state of flow.

On the bottom: decrease of pressure from the stagnation point lying far in front, acceleration of the flow particles, thin friction layer, favorable drag effect of the external flow; the friction resistance is easily overcome by the particles nearest the wall; no detachment of flow.

In the direction of the span: the flow particles wander to the region of lowest underpressure, and specifically to a greater extent, the lower the velocity, they thicken the friction layer there and

therefore promote the detachment. With the detached flow the area of maximum underpressure is on the edge of the "dead water". Particles of the friction layer of the neighboring region with attached flow, but also of the region of separated flow, are sucked into this low pressure region. This causes an extension of the region of separated flow.

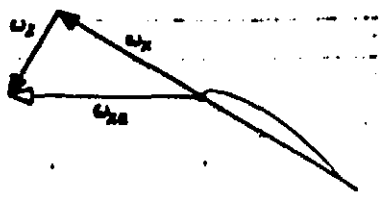

Fig. 10. Decomposition of flow fixed vector $\omega_{x\alpha}$ in the corresponding wing fixed partial vectors ω_x and ω_z.

Through the centrifugal acceleration particles nearest the wall are driven from the interior against and over the edges of the wing. In case of flow firmly applied on all sides, no special importance need be attributed to the acceleration effect even for high rotation values. On the other hand with the start of the detection they appeared to assume a decisive effect on the nature of the flow.

To consider the coriolis effects let the wing be compared as regards the wing fixed z axis as a disk rotating with the angular speed ω_z, see Fig. 10.

Since right hand rotation was selected for the wing, the coriolis acceleration is manifested in a left hand rejection of the flow (left hand: from an observer rotating at the same time and looking in the direction of the relative movement). Thus for example a relative movement forced outwardly by pressure gradient in the span direction on the upward moving airfoil half causes a driving of the flow against the rear edge of the wing, on the right hand wing half against the wing leading edge, accordingly, on the left a deflection in a dirction promoting the application of the flow, in the right hand side a direction promoting detachment. In the direction of depth the deflection

takes place on the left inwardly, on the right outwardly. It may be assumed that the coriolis acceleration affecting the entire airfoil flow does not play any role at all for very small angles of attack and for the rotation values occurring usually. For very high angles of attack and also when the flow is located in the transition from the attached to the separated state, it may be important, say in the transition for sharp spin flight ($\alpha_0 \approx 30°$; $\lambda = 0.35$) or in the flat spin flight ($\alpha_0 \approx 50°$; $\lambda \approx 0.6$).

In the following discussion of the measurement results, we refer to the individual effects described above from case to case.

8. Discussion of the Results of Theory and Experiment

a) Airfoil 1, straight rectangular wing $\lambda = 0$ (Figs. 11-14).

The pressure distribution curves for these wings (Figs. 11 and 12) show for very small angles of attack on the top and bottom basically the variation to be expected for the study profile. Naturally we should note the low pressure regions over the rear portion of the top of the wing in the boundary region. They have also been established in other measurements and must be attributed to the strong flow around the wing edges which have a sharp shape here.

The parameters obtained by integration along the depth and span for the average normal force of the wing $\overline{c_n}$ were plotted in the diagram of Fig. 14. They are very consistent with the values of the measurement of force except for the values in the region of the decrease of buoyancy. To explain these differences it should be stated that in this c_a region it is only rarely possible to obtain the flow forced to be reattached by "stalling" of the wing in the wind tunnel for the duration of a pressure distribution measurement

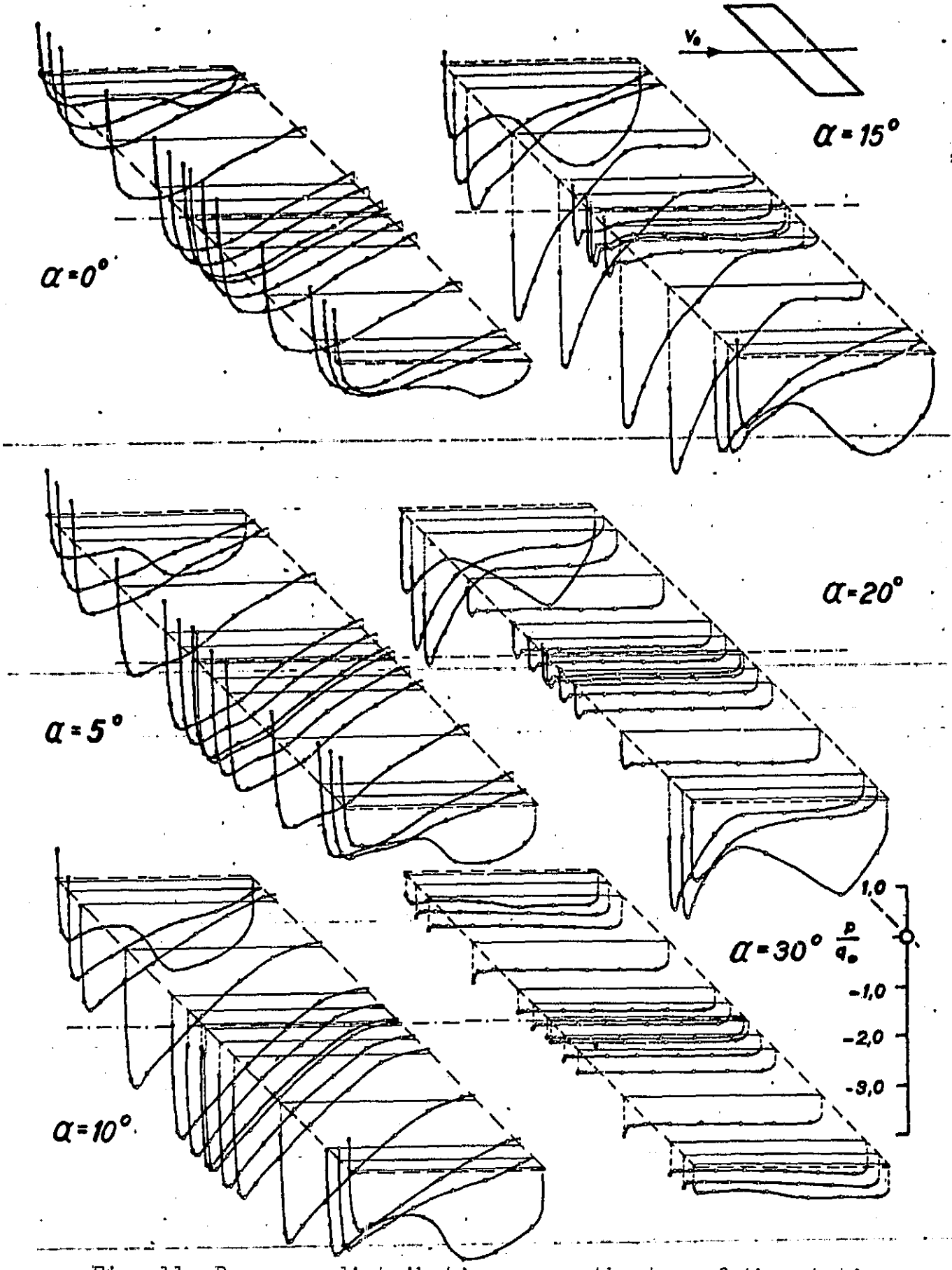

/163

Fig. 11. Pressure distributions over the top of the stationary airfoil 1 for different angles of attack.

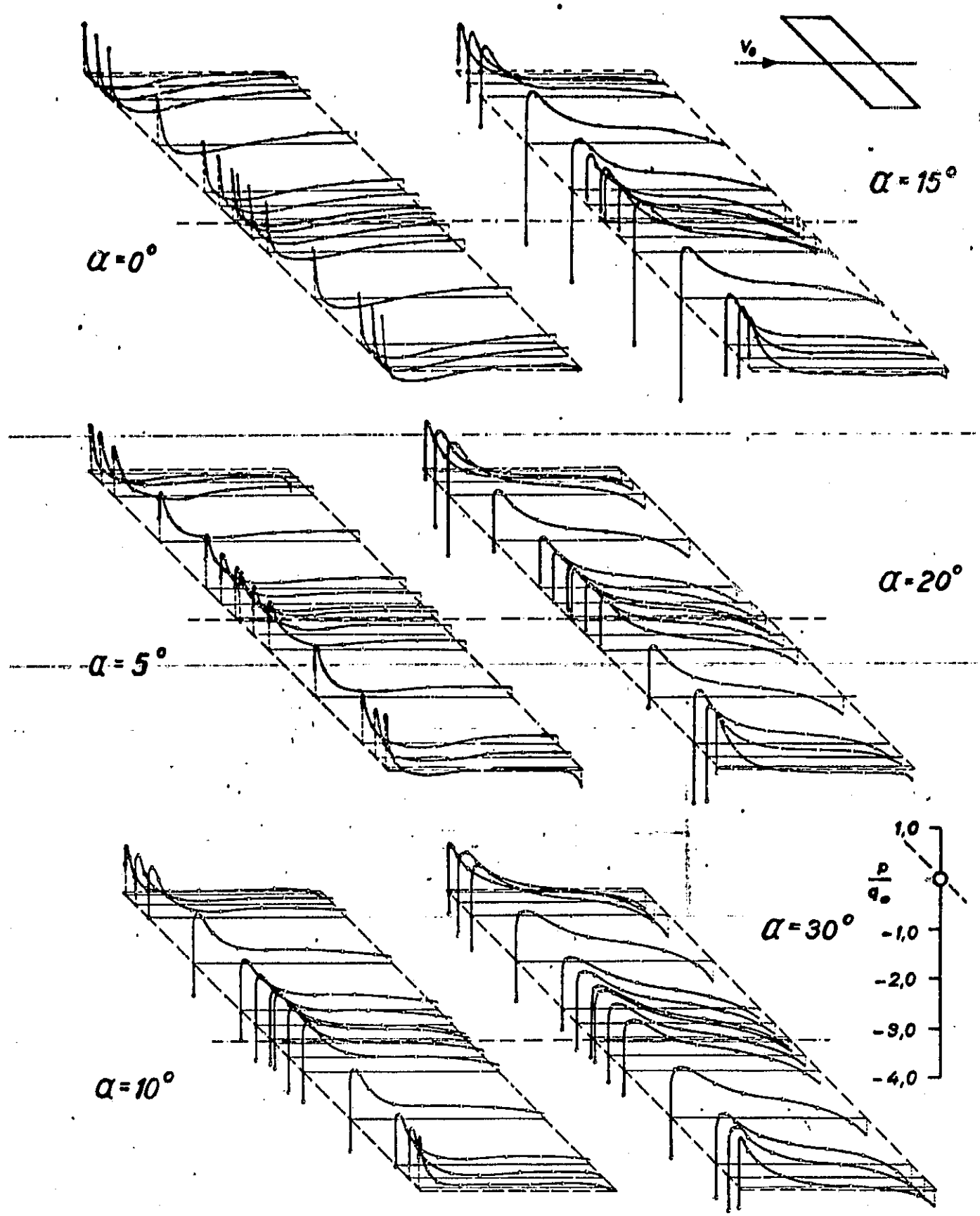

Fig. 12. Pressure distribution over the bottom of the stationary airfoil 1 for different angles of attack.

in this state, the more so because even small pressure borings (diameter 0.5 mm), even with the most careful execution present gaps for the flow mechanism highly sensitive in this area.

In several repeated tests it was possible always for $\alpha=15°$ to determine the pressure distribution in the stalled state and thus fix for measurement purposes the beginning of separation of the flow for the rectangular wing, Figs. 11 and 13. In this connection it is surprising that the narrow strip of totally separated flow was able to remain in the wing center near the region of flow least attached in the front part of the wing. Signs of detachment are also shown by the sections lying in the center of the half span. Unseparated flow dominates only in the section near the edge. For $\alpha=20°$, the "dead water region" has already become much wider and the pressure distribution lying over the section far outside shows the above indicated total detachment. This is achieved for $\alpha=30°$; even low pressure regions in the neighborhood of the wing edge have collapsed

/165

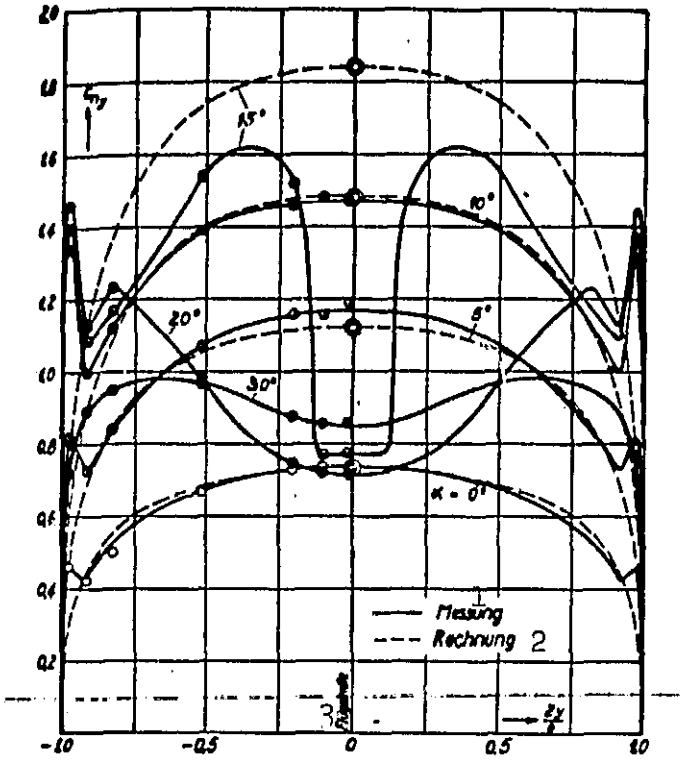

Fig. 13. Experimental normal force distribution for the stationary airfoil 1 for different angles of attack and comparison with the calculated buoyancy distribution.

Key: 1. Measurement; 2. Calculation; 3. Wing spin

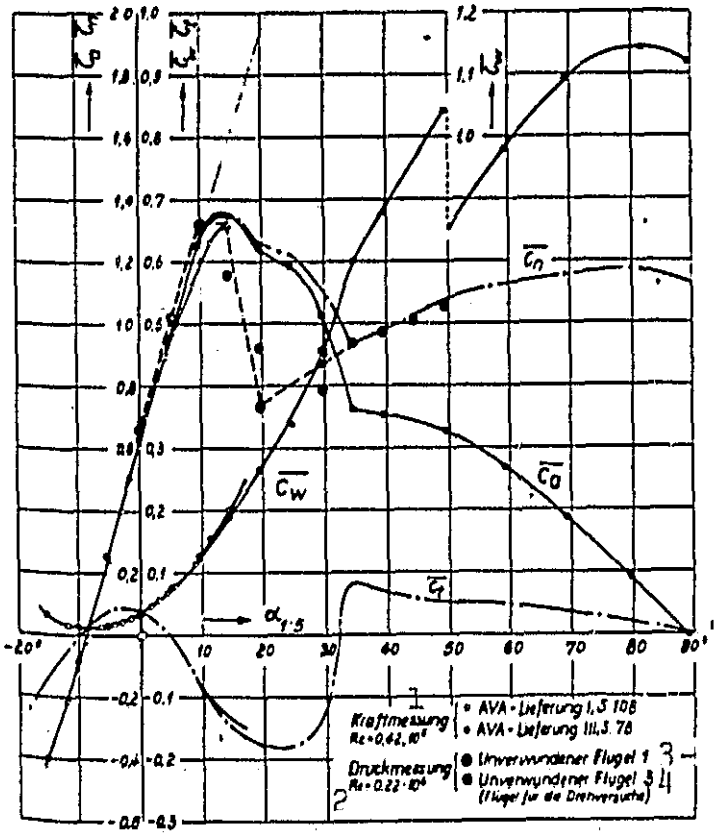

Fig. 14. Results of measurments of force and pressure on the airfoil with the Göttingen 420 profile and the aspect ratio 1:5.

Key: 1. Measurement of force.
2. Measurement of pressure;
3. Untwisted wing 1; 4. Untwisted wing 3 (wing for rotation tests)

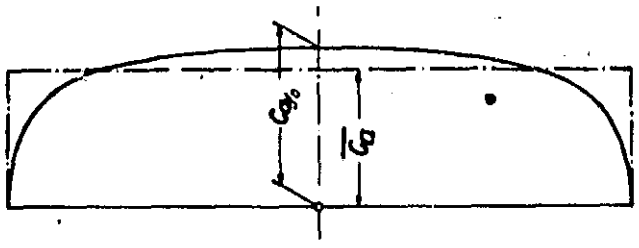

Fig. 15. Definition sketch for $\overline{c_n}$ and cn_{y0}.

on themselves, Fig. 11. For fiber probe observations the degree of separation because of the disturbing effect of the probe is always larger than for the measurements themselves.

The flow on the bottom of the wing does not show any extraordinary behavior for all the angles of attack studied. It seems to be hardly influenced by the processes on the top of the wing, Fig. 12.

The results of calculation and measurement are compared with each other in Fig. 13. The following may be mentioned on the assignment of the curves:

The theory gives the basic distribution for the angle of attack. The buoyancy distributions of the different angles of attack are now related

to this basic distribution. The criterion of affinity is determined for the buoyancy coefficient of the wing center c_{ay0}. In this connection the average buoyancy coefficients $\overline{c_a}$ are taken from Fig. 14 for the angle of attack concerned and provided with the wind tunnel correction, and multiplied by the value of the ratio of the theoretical buoyancy coefficient in the center of the wing c_{ay0th} on the theoretical average buoyancy coefficient $\overline{c_{ath}}$.

$$c_{ay_0} = \overline{c_a}\left(\frac{c_{ay0th}}{\overline{c_{ath}}}\right).$$

Starting from this value c_{ayo} then the development of the calculated buoyancy distribution was carried out, while we still assume $c_{ay}=c_{ny}$, Fig. 15.

Fig. 13 shows for very small angles of attack considerable consistency between the calculated and experimental results, in spite of somewhat disturbing buoyancy peaks at the wing edges. For larger angles of attack, say starting from $\alpha=15°$, however considerable differences occur, which become incompatibly large with further increase of the angle of attack. For these angles of attack, the flow is no longer able to follow the wing profile, it is detached and thus loses the nature which it had assumed according to the thoery.

b) Airfoil 2, twisted rectangular wing.

Twists according to $\lambda=0.3$ (Figs. 16, 17, 18).

The twist is equivalent to a rotation to the right, therefore rectilinear increase of the angle of attack from left to right. The extent of the change may be seen on Fig. 19 for $\alpha_0=15°$.

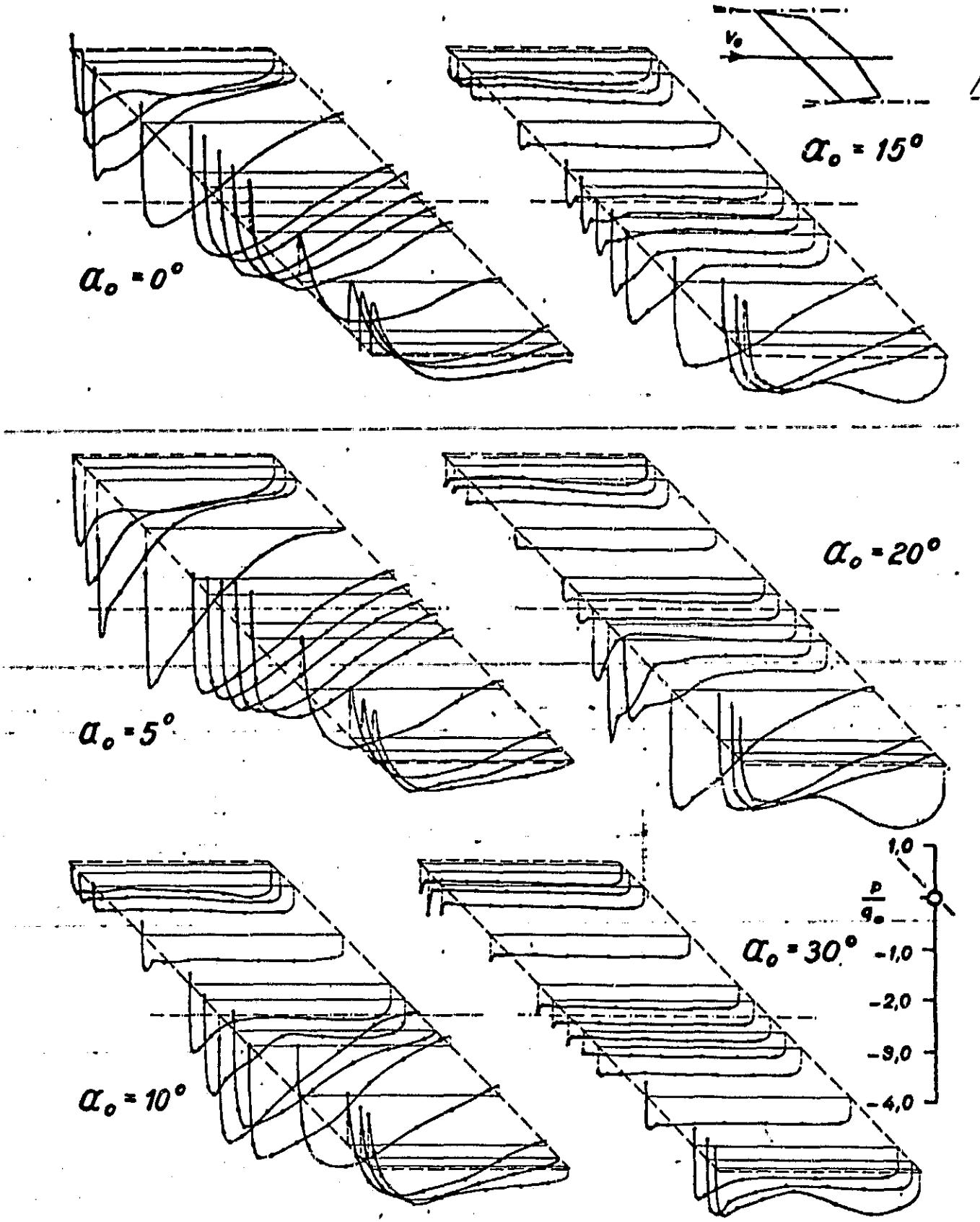

Fig. 16. Pressure distributions over the top of the twisted airfoil 2 for different angles of attack.

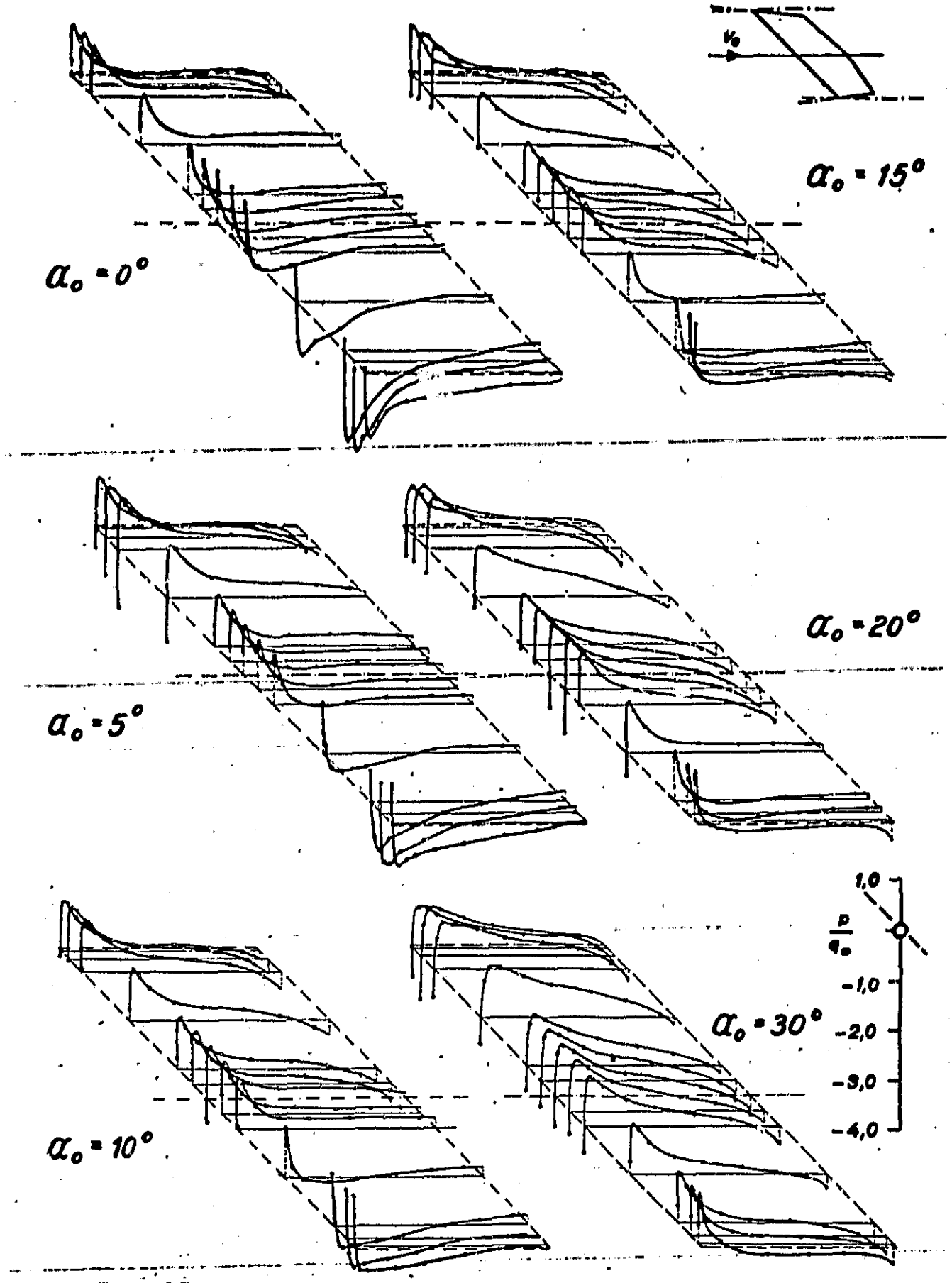

Fig. 17. Pressure distributions over the bottom of the twisted airfoil 2 for different angles of attack.

Fig. 18 gives a comparison between the calculated and experimental studies. The calculated values are obtained from the distribution of the untwisted wing and from the component of twisting by superimposition, Fig. 20. The key value here was c_{ny0} of the straight airfoil, that is c_{ny0} (straight wing)=c_{ny0}(twisted wing). This, as also shown by the measurements (normal forces Fig. 18, pressure distribution Fig. 21),is permissible for totally attached flow, since the eddy proceeding backwards from the airfoil halves induces in the wing center additional angles of attack of the same value, but of opposite sign. /168

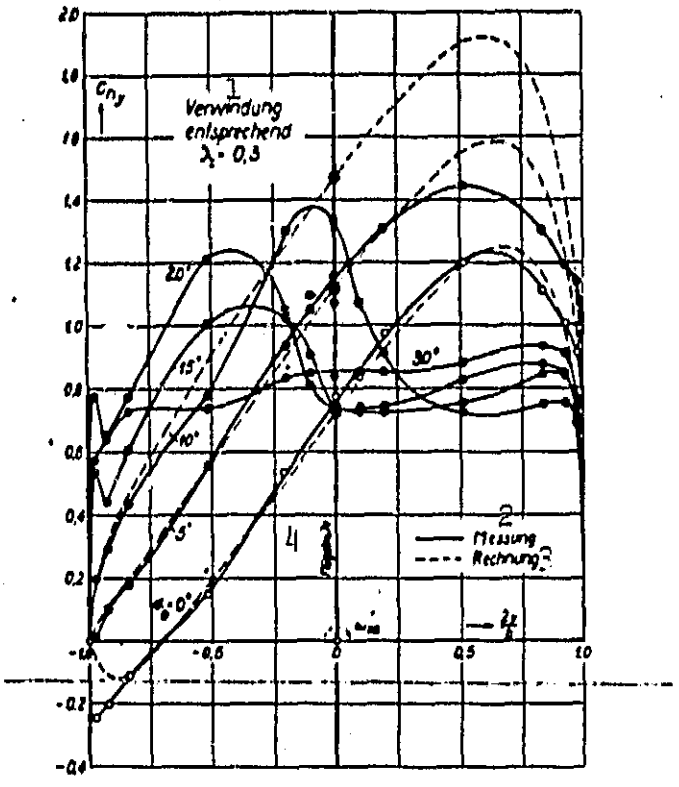

Fig. 18. Experimental normal force distribution for the twisted airfoil 2 for different angles of attack in comparison with the computed buoyancy distribution.

Key: 1. Twisting according to λ=0.3;
2. Measurement; 3. Calculation
4. Wing center

Calculation and experiment give results which are very consistent for attached flow, Fig. 18. For α_0=5° laterally the beginning of the detachment over the strongly loaded section of the right hand half of the wing can already be recognized. For α_0=10° then the flow on the top assumes the form which exists in the tilting over the end of the wing. The differences in the calculated and the experimental values are already quite large here. For α_0=15° and 20°, the asymmetry of normal force distribution

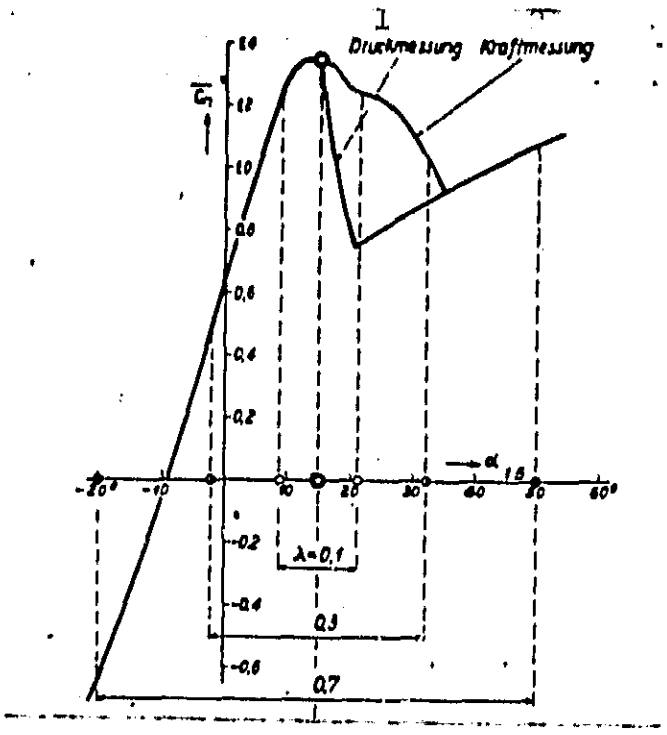

Fig. 19. Range of variation of the geometrical angles of attack as a result of the rotation, indicated for a_0=15° and some values of rotation.

Key: 1. Measurement of pressure; 2. Measurement of force.

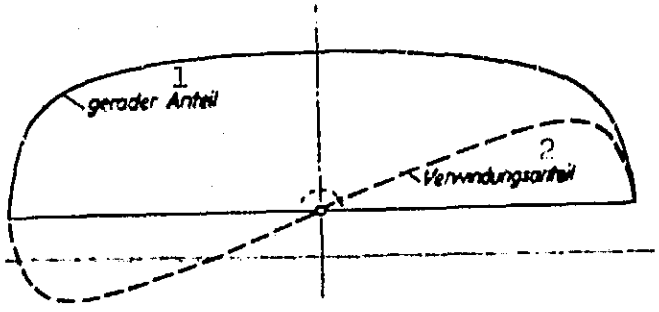

Fig. 20. Schematic representation of the system twisted or rotating in the same direction along the span for the buoyancy distribution of effective components.

Key: 1. Straight component; 2. Twisted component

has progressed to such an extent that even the wing left behind is put into self rotation. A consistency between calculation and experiment can no longer be expected here at all, since the "dead water" of the top flow has already become too wide. This applies actually only to α_0=30°, when on the top of the wing only totally separated flow may be found. The pressure distribution of the bottom does not show any unusual variation. It provides a momentum with backward rotation increasing with the angle of attack. The comparison with the rotating airfoil 3 is discussed in the following section.

c) Airfoil 3, straight rectangular wing with rotation (Figs. 22 to 32).

The investigation started for α_0=15°. The measurement for very low angle of attack did not seem to be advisable in view of the high

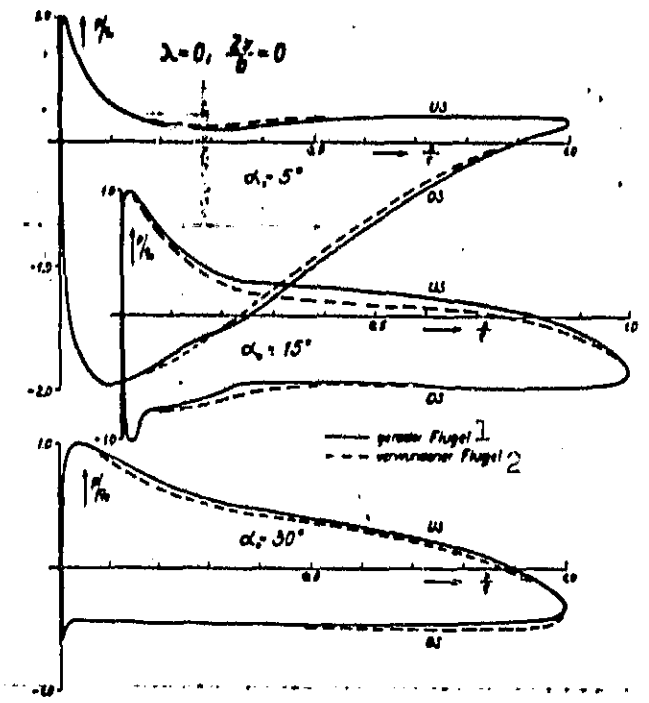

Fig. 21. Comparison of the pressure distribution in the direction of depth over the central section.
a) of the straight airfoil 1,
b) of the twisted airfoil 2 for several angles of attack.

Key: 1. Straight wing; 2. Twisted wing

rotation values of the chosen type of model attachment, since one had to expect a considerable disturbance of the flow in the center of the wing because of the holding rod of the model. From α_0=15° onward this rod is, however, on the separated flow portion of the top, so that from then onward its effect may be considered as insignificant.

The average normal force coefficient $\overline{c_n}$ determined from the pressure distribution for λ=0 are, according to Fig. 14, somewhat lower than those of airfoil 1. This can /169 be attributed, besides the already discussed difficulties, in the "stalling" of the model in the wind tunnel, to production precisions, the wing 3 hammered in plate should be (particularly in the region of the wing nose difficult to shape) larger than for wing 1.

From the measurement results with the rotating airfoil 3, the following should be emphasized:

For α_0=15° (Figs. 22, 23, 24) positive rolling damping still exists for λ=0.1 and 0.2. For λ=0.1 however, a certain unsteadiness is found in the depth distribution of the pressures over the external sections of the top of the right hand half of the airfoil,

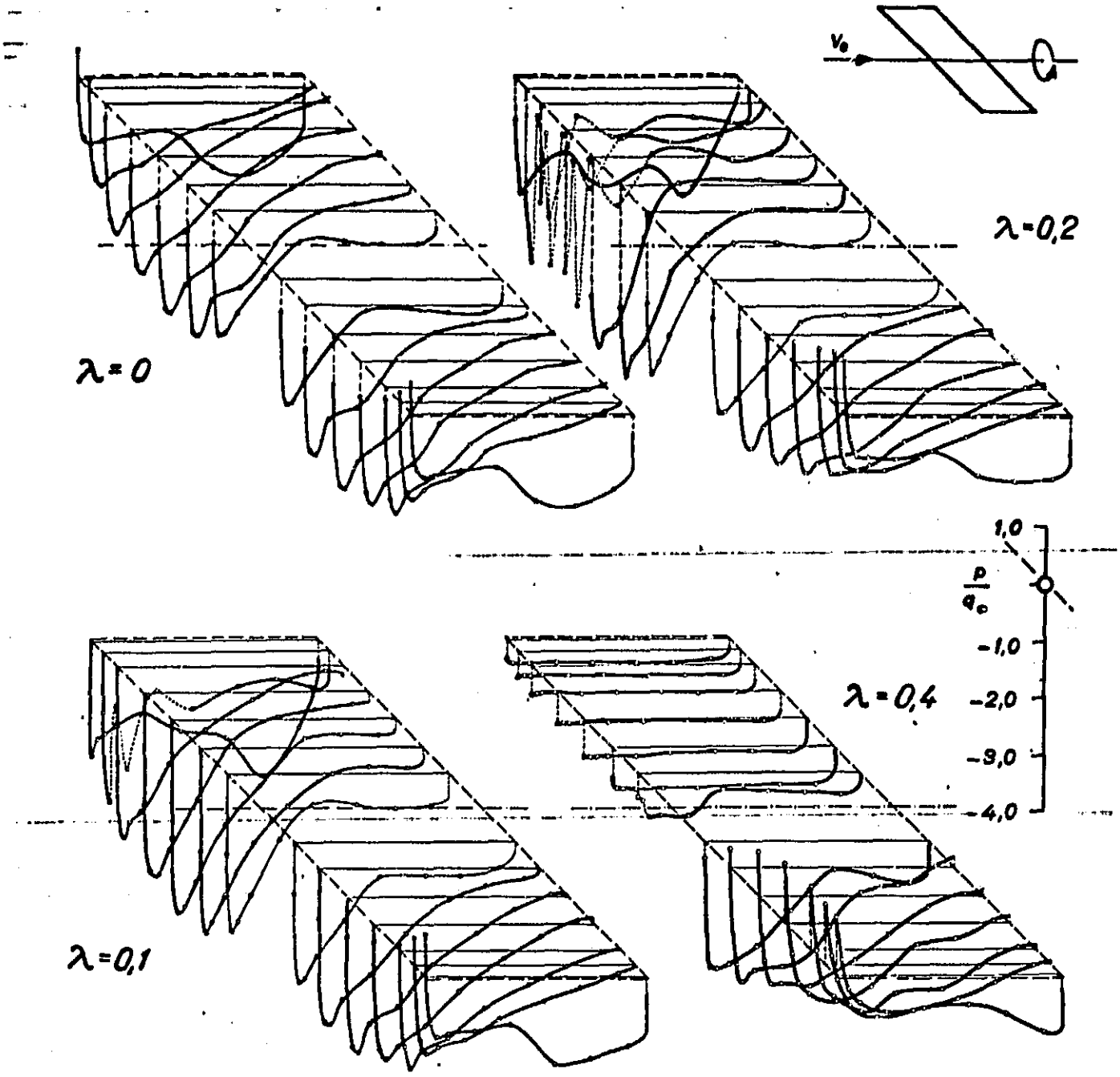

Fig. 22. Pressure distributions over the top of the rotating airfoil 3 for the angle of attack α_0=15° for different values of rotation.

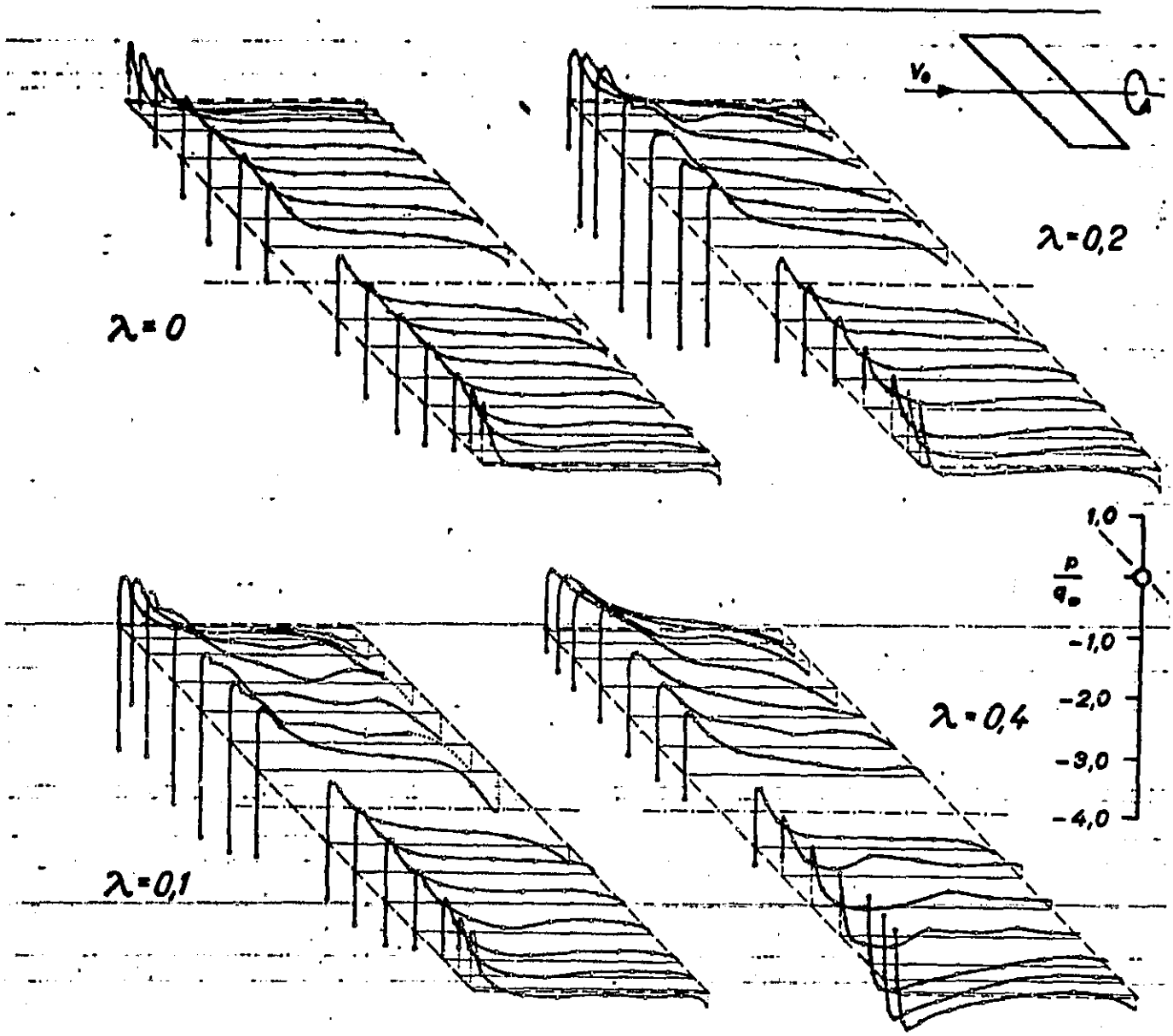

Fig. 23. Pressure distributions over the bottom of the rotating airfoil 3 for the angle of attack $\alpha_0=15°$ for different rotation values.

increasing for $\lambda=0.2$. For $\lambda=0.4$, the flow on the top assumes specifically the nature of a distribution leading to self-rotation, since the flow lies on the left hand side, that is the upward half of the wing; on the right hand side it is separated. But the

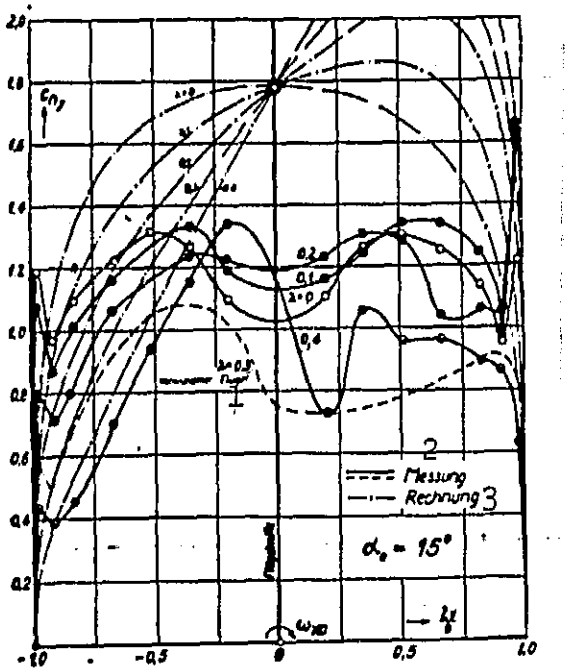

Fig. 24. Normal force distribution over the airfoil 3 for an angle of attack α_0=15° for different rotation values and attempt at comparison with the values obtained by calculation.

Key: 1. Twisted wing; 2. Measurement; 3. Calculation

self-rotation, as indicated later on the basis of Fig. 35, does not occur any longer, since the load on the top of the left half of the wing has already decreased very much because of the relatively high rotation values and the effect of the bottom, which always contributes to the momentum of backward rotation, has increased.

For α_0= 15°, an attempt was also made to calculate the buoyancy distribution for several values of rotation, Fig. 24. In this connection it was assumed that the flow is still completely attached and $\frac{d\overline{c_a}}{d\alpha}$ has maintained a value valid for the attached flow. /170

The distribution curve was developed just as in the case of the airfoil 2, from the value c_{nyo}, which was obtained from $\overline{c_a}$ obtained by rectilinear extrapolation of the $\overline{c_a}$,α curve, Fig. 14 for the angle of attack provided with the wind tunnel correction. For very low rotation values, the consistency is poor as expected. Only for very large λ it improves on the left hand half of the wing with attached flow, while it deteriorates even further on the right half of the wing.

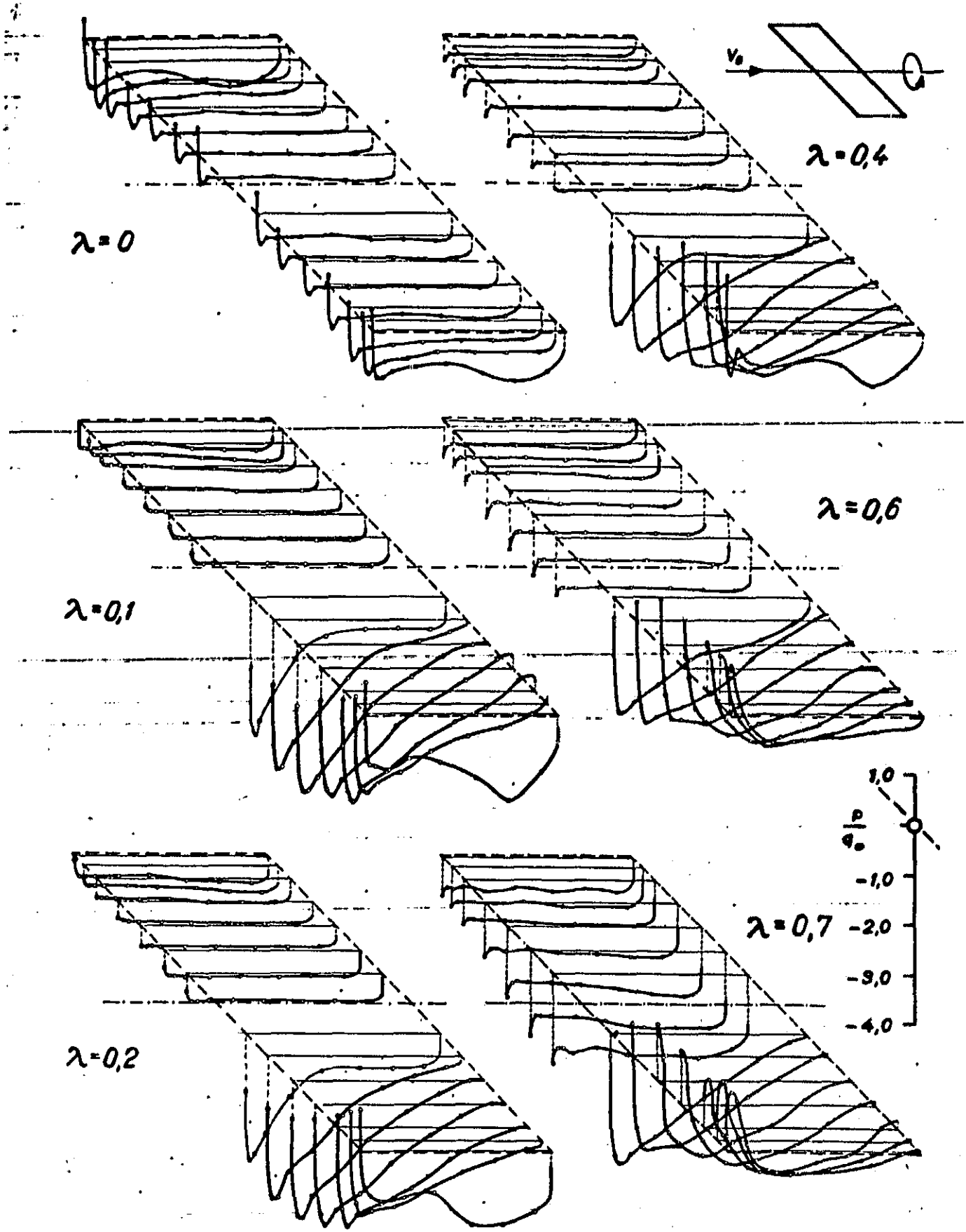

/171

Fig. 25. Pressure distributions over the top of the rotating airfoil 3 for the angle of attack α_0=20° for different values of rotation.

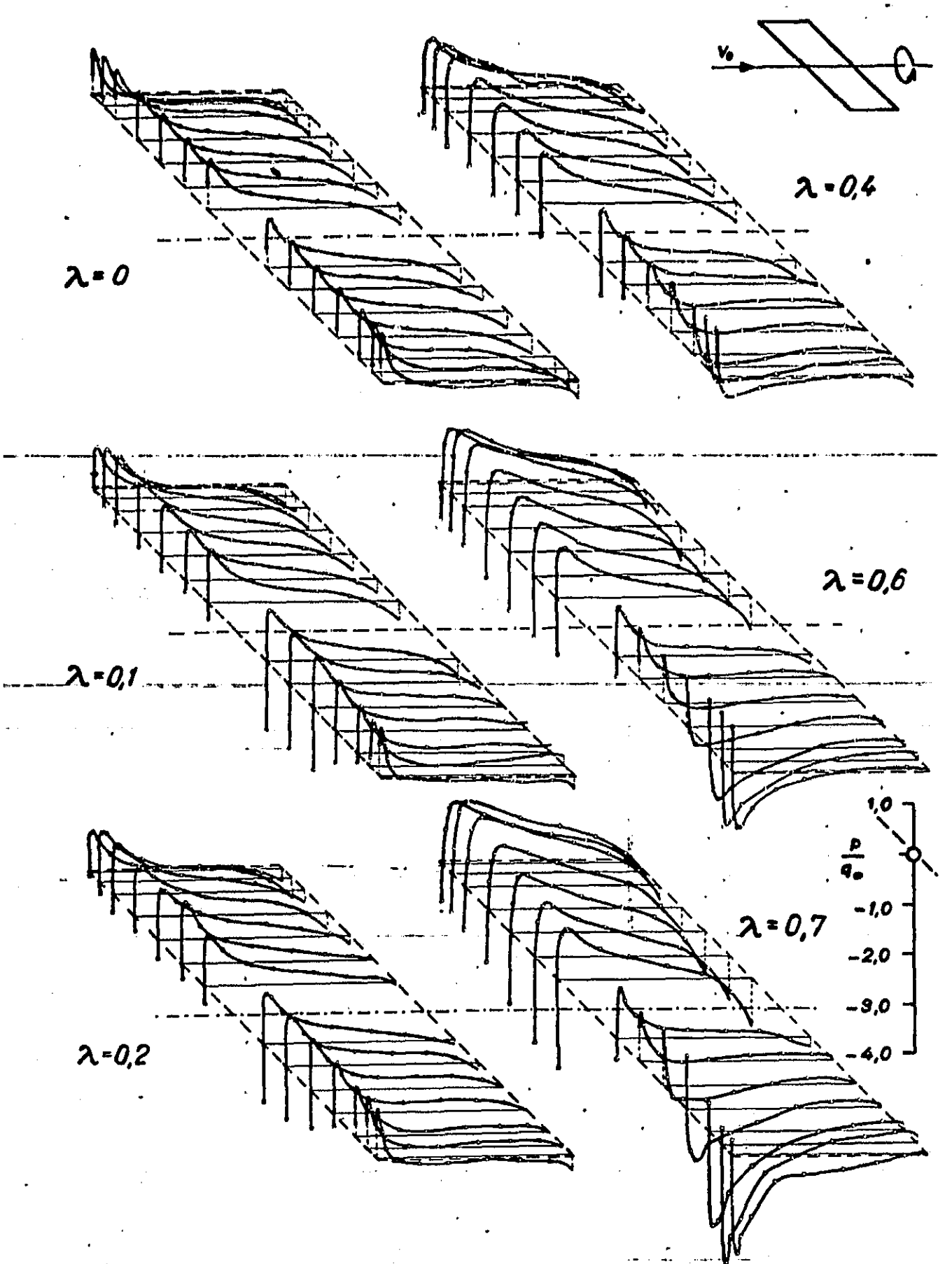

/172

Fig. 26. Pressure distributions over the bottom of the rotating airfoil 3 for the angle of attack $\alpha_0=20°$ for different values of rotation.

For α_0=20°, Figs. 25, 26, 27, the pressure distribution for λ=0.1 and 0.2 predominates, and therefore the normal force distribution, as may be found on the self rotating airfoil at the beginning of the rotation. The top has the strong asymmetry of distribution in the sense of the propulsion. The distribution of the bottom arising in the direction of backward rotation cannot provide here a full compensation. The case is that the self-rotation occurs from the state of totally separated top flow through reattachment to the upward half of the wing. But more frequently the autorotation takes place from the state only partly, /175
but symmetrically separated top flow by further separation on the downward half of the wing. This process can be expected for the wing concerned between α_0=15° and 20°, and is completed on top, say at α_0=15° and λ=0.4.

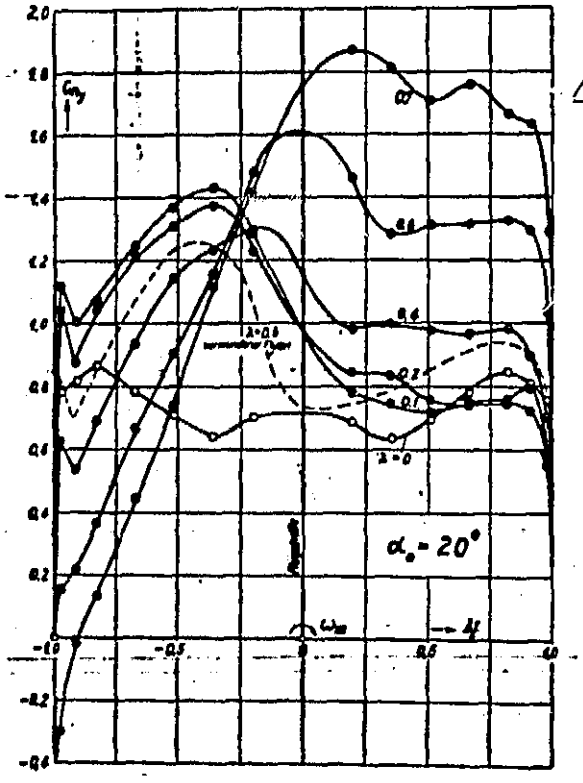

/170

Fig. 27. Normal pressure distribution over the airfoil 3 for an angle of attack α_0=20° for different values of rotation.

For α_0=30°, Figs. 28, 29 to 32, the flow on the wing at rest is naturally separated over the entire top of the wing. Small values of rotation do not cause much change in this distribution. Only for very high values of rotation phenomena may be observed which make it necessary to have a more thorough consideration.

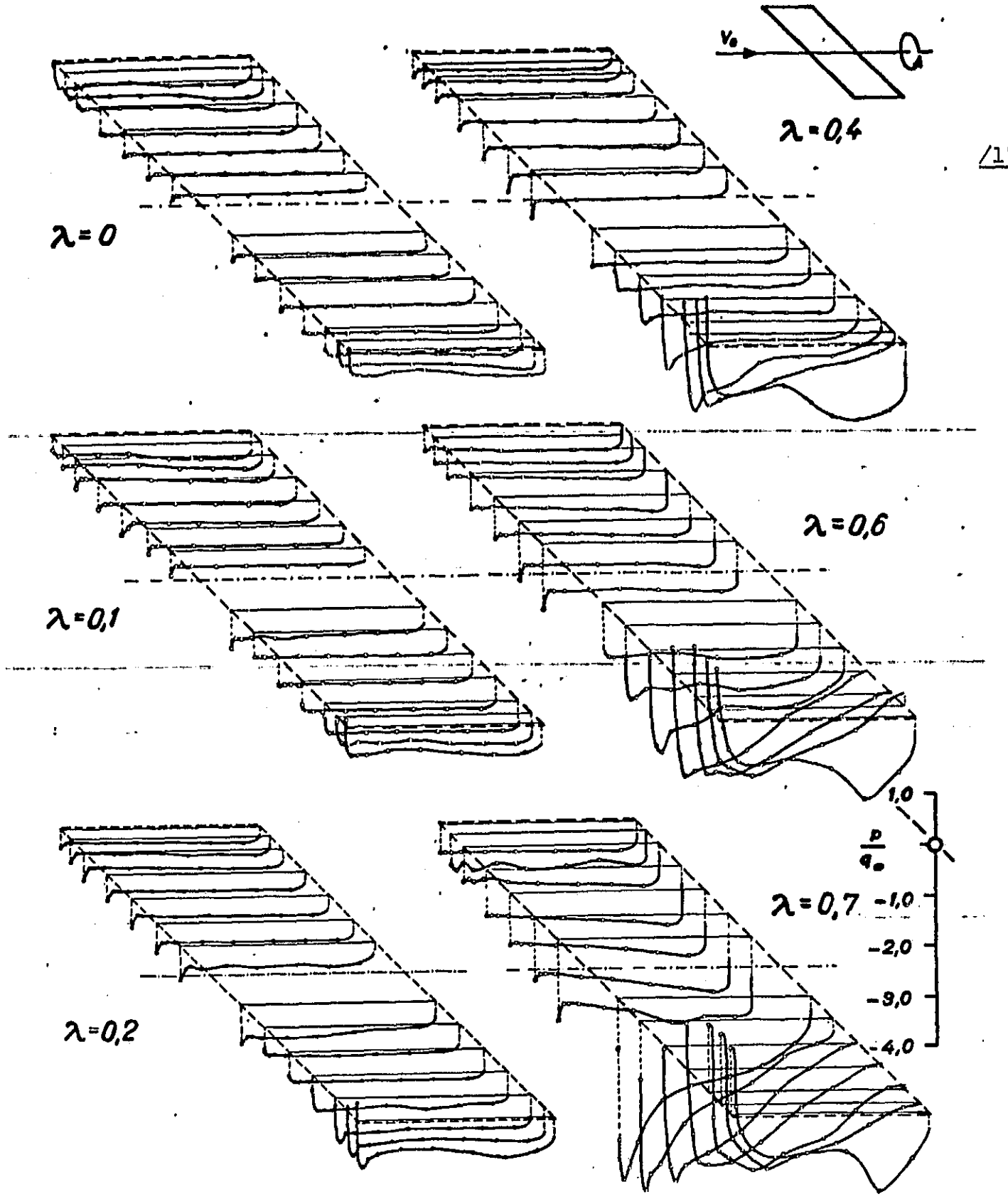

/173

Fig. 28. Pressure distribution over the top of the rotating airfoil 3 for the angle of attack $\alpha_0=30°$ for different values of rotation.

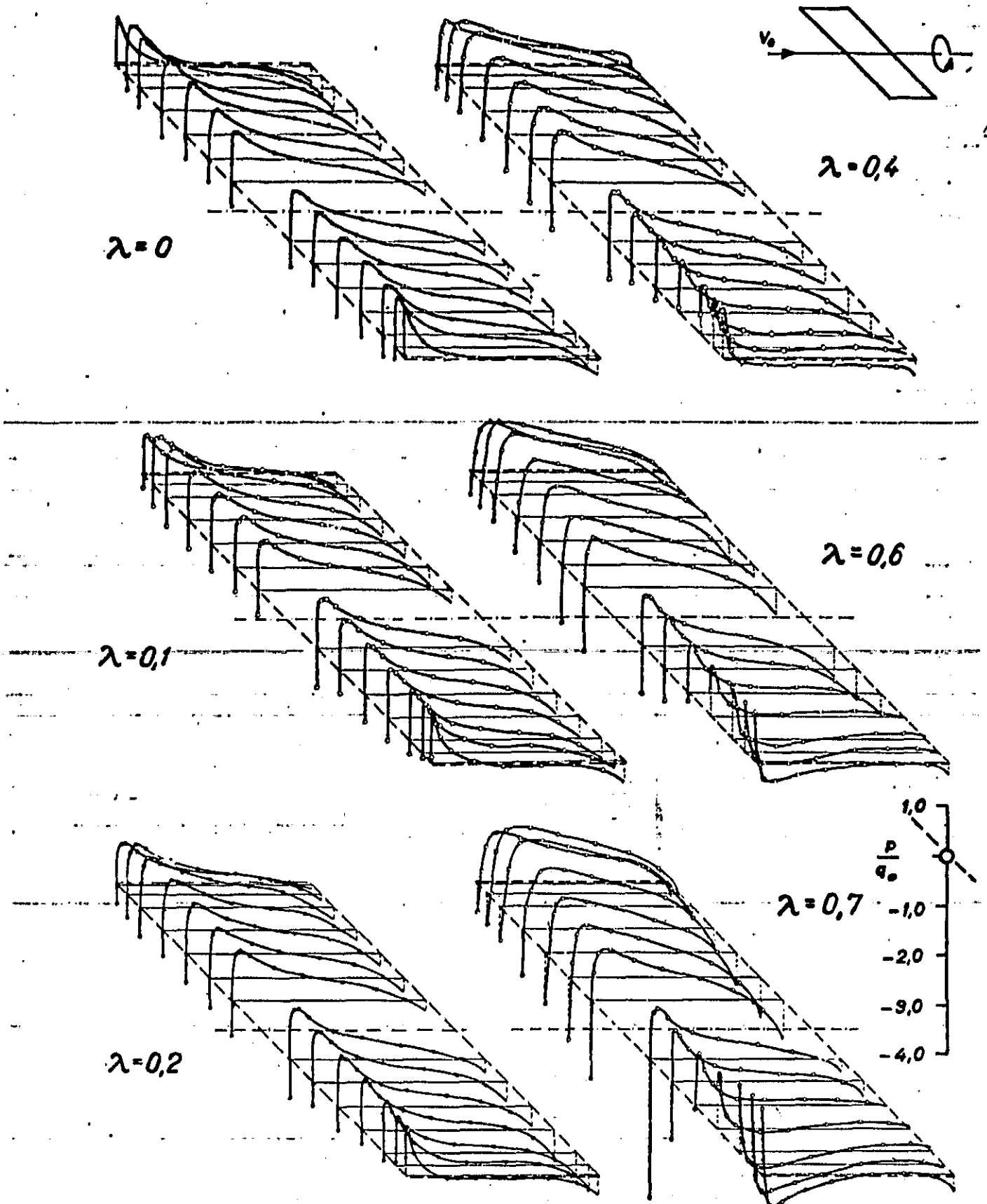

/174

Fig. 29. Pressure distributions over the bottom of the rotating air foil 3 for the angle of attack $\alpha_0=30°$ for different values of rotation.

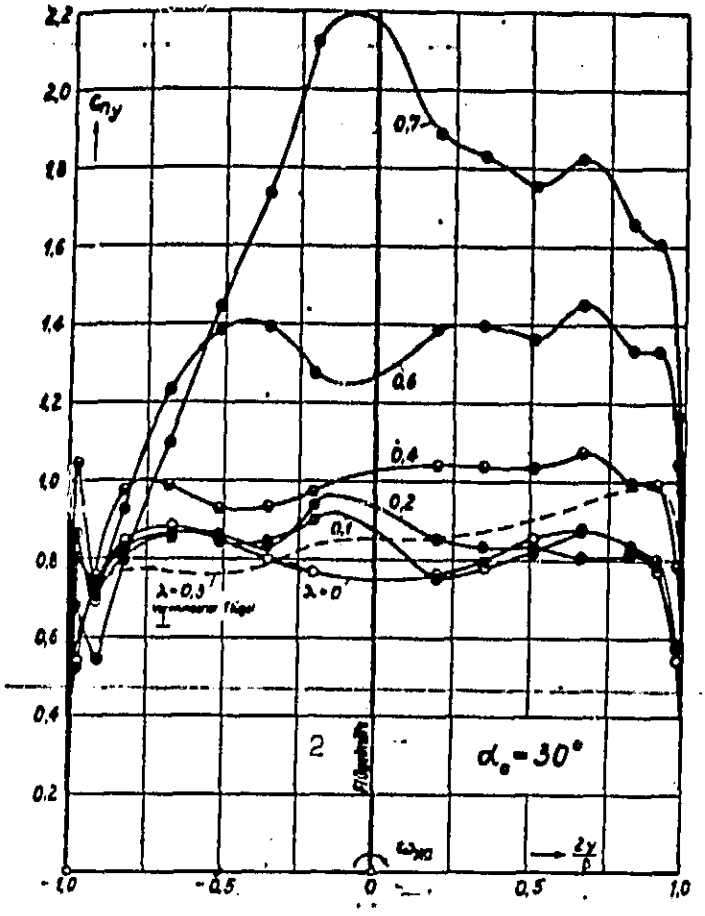

Fig. 30. Normal force distribution over the airfoil 3 for an angle of attack $\alpha_0=30°$ and for different values of rotation.

Key: 1. Twisted wing; 2. Wing center

These phenomena also occur for $\alpha_0=20°$, and specifically for values of rotation $\lambda>0.3$. We consider the following:

1. that in the attached part of the flow c_{ny} values occur which are much higher than the larger c_{ny0} value measured for $\lambda=0$;

2. that in the separated part of the flow the c_{ny} values on the downward half of the airfoil are rather high and assume moreover almost uniform values.

In this connection the following may be stated:

1. If the flow were attached at all sides, then for the rotation values, according to theory, fairly high c_{ny} values should be expected, as may be seen for example in Fig. 24 for $\alpha_0=45°$. Therefore it should be assumed with certainty that the above described effects of the forces of inertia, especially centrifugal force, would result in a reattachment of the flow over the sections

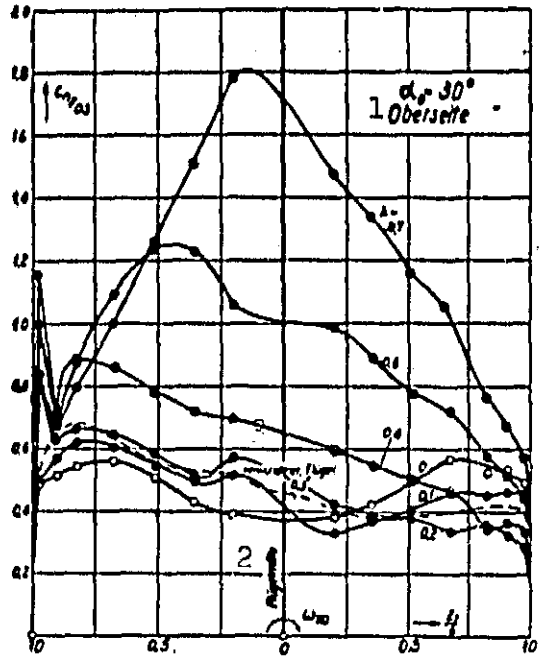

Fig. 31. Component of the top in the normal force distribution on airfoil 3 for an angle of attack $\alpha_0=30°$ and for different values of rotation.

Key: 1. Top; 2. Wing center; 3. Twisted wing

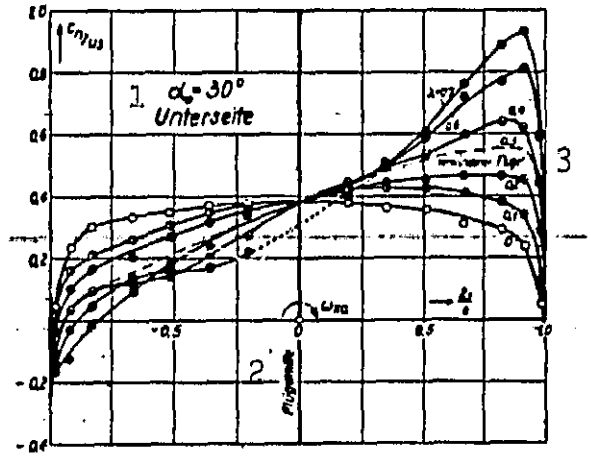

Fig. 32. Component of the bottom in the normal force distribution over airfoil 3 for an angle of attack $\alpha_0=30°$ and for different values of rotation.

Key: 1.Bottom; 2. Wing center; 3. Twisted wing

lying further in on the upward top of the wing, and thus allow the approach to the theoretically expected values of c_{ny}. At the same time the relatively high underpressure over the neighboring region with separated flow appears to affect the attached flow and to shape the pressure distribution more completely in its rearward portion. With $\lambda=0.7$ the largest measured c_{ny} value is for $\alpha_0=20°$ at 1.85, for $\alpha_0=30°$ at 2.2, while it amounts to 1.55 for the straight nonrotating wing.

2. The increase observed for $\lambda>0.3$ for c_{ny} on the downward half of the wing occurs because of a decrease progressing with λ of the underpressure on the top and an increase of the overpressure on the bottom. The processes on the top may be determined by the underpressures over the flow applied to the front portion of the border region, while the increase of pressure over the bottom may be attributed to the wandering of the stagnation point towards the rear edge of the wing, connected with the

local increase in the angle of attack. To reveal more clearly the components of both sides of the wing, for $\alpha_0=30°$ as an example, the c_{ny} values of the top and bottom are shown separately, Figs. 31 and 32.

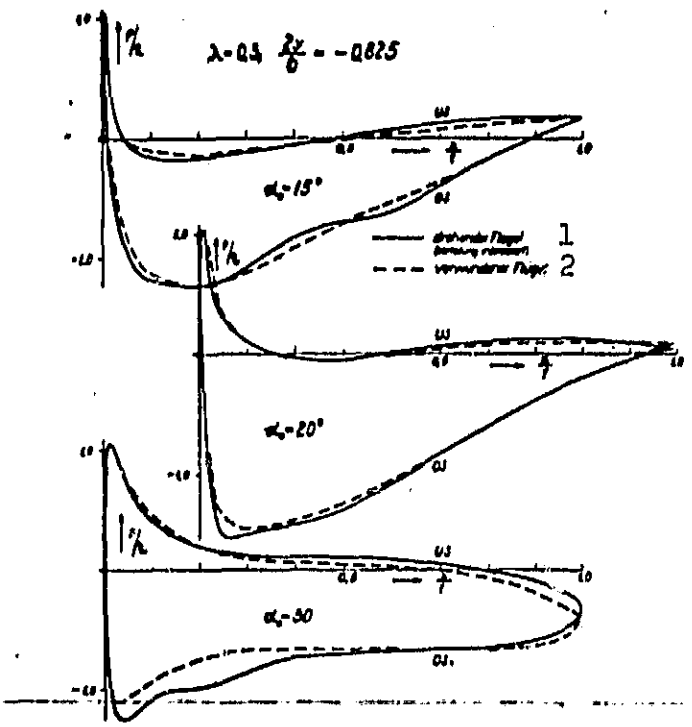

Fig. 33. Comparison of the pressure distribution in the direction of depth over a section lying on the left, that is on the upward half of the wing.

a) for the twisted airfoil 2;
b) for the rotating airfoil 3 for different angles of attack α_0.

Key: 1. Rotating wing (interpolated solution); 2. Twisted wing

The curves of the /176 normal force coefficient c_{ny} of the twisted airfoil 2 corrected with $\frac{qy}{q0}$ are very consistent, as may be seen from Fig. 24, 27, 30 to 32, for attached flow and even with separated flow still fit in to some extent satisfactorily in the family of curves corresponding to the rotating wing. The same may be seen also for the pressure distribution measurements, Figs. 33 and 34, which were taken for comparison from the large number of measured distributions.

In the transition regions from attached to separated flow, the consistency is still valid for the basic variation of the curve $c_{ny}=f(\frac{2y}{b})$, but hardly for the other values.

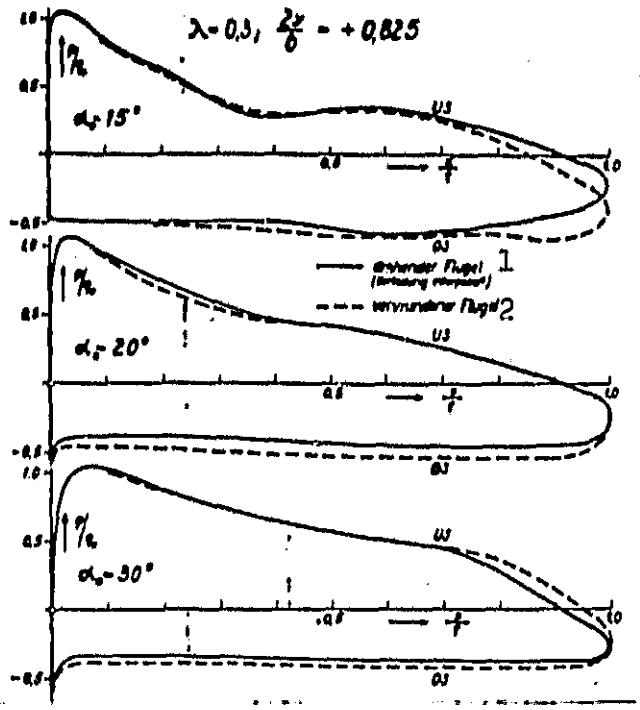

Fig. 34. Comparison just as in Fig. 33, but for a section lying on the right hand side, that is on the downward half of the wing for different angles of attack α_0.

Key: 1. Rotation wing (interpolated distribution); 2. Twisted wing

Finally the coefficient c_{Lx0} of the angular momentum around the axis of rotation x_a of the system are plotted as a function of the angle of attack α_0. The values are obtained by forming the difference of the partial movement of the left and right halves of the wing.

Since the values of these partial movements differ only a little from each other, here the requirement for the precision of the results should not be taken too high. Nevertheless, this figure shows the self rotation region coming into consideration for the studied airfoil, whose extent is satisfactorily consistent with the ones known from earlier experiments.[13]

9. Summary

1. As long as the flow on the airfoil is firmly attached on all sides, the airfoil theory gives results which are very consistent with the measured ones even for relatively high buoyancy coefficients. It was possible to show this for the airfoils moving precisely

---

[13] See footnote 3b.

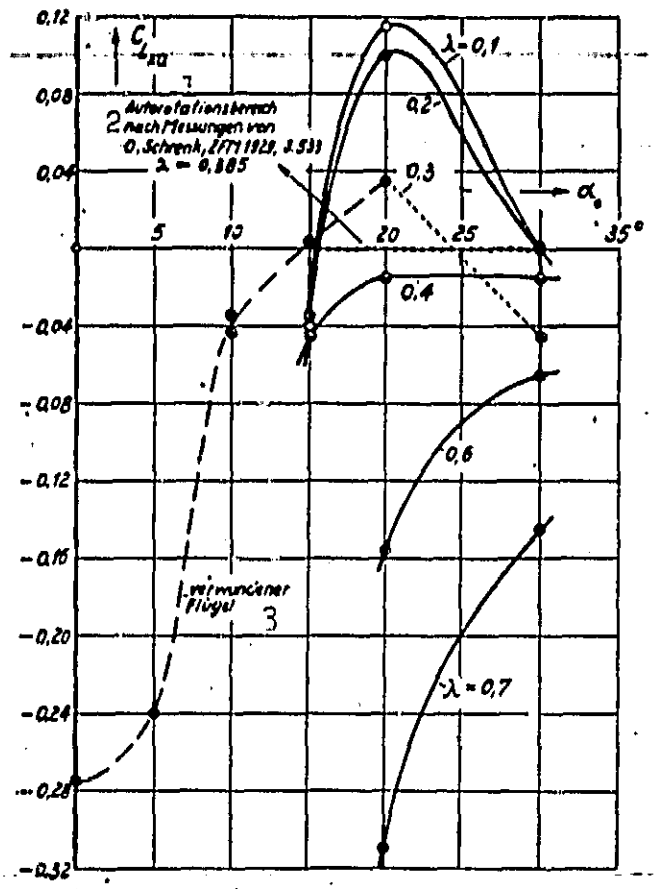

Fig. 35. Coefficient c_{Lxa} of the angular momentum of airfoil 3 around the longitudinal axis x_0 fixed with regard to flow for different values of the coefficient λ depending on the angle of attack α_0. The values of the twisted airfoil 2 are introduced for comparison.

Key: 1. Self rotation range; 2. According to the measurements of; 3. Twisted wing

parallel to themselves and for the airfoil twisted for a certain value of rotation and as may be derived from the comparison of pressure distributions, applies also for the rotating airfoil for practically all values of rotation occurring.

2. If however, the flow is in a state of transition from the attached to the separated state, then, as taught by experience, its sensitivity to disturbing effects increases. In this case the effects in the direction of the span become more important, whether it is as a result of pressure gradient forces, or in the rotating wings as a result of the /177 forces of inertia. For values of rotation $\lambda > 0.3$, considerable increases occur in the amount of the local normal force coefficients, which allow the conclusion that the forces of inertia have special influence. As a result of the centrifugal acceleration, particles of the friction layers are driven out from the internal wing section.

This promotes the application of the flow over the wing. For larger angles of attack under certain conditions, the coriolis accleration may also have an effect on the flow favoring the attachment, especially when the flow is in the above-indicated transition state. To further clarify this relationship, a thorough study of the naturally very complicated spatial processes in the friction layer is necessary.

3. For completely separated flow the rotation seems to have no special effect on the flow processes on the wing, as long as the rotation values remain low. For $\lambda=0.3$, the differences between the untwisted and rotating wings are still of a size which is mutually compatible. For larger rotation values, however, a considerable increase may be observed in the local normal force coefficient, which must be attributed to the forces of inertia.

4. The existing pressure distributions give a deeper insight into the flow processes on rectangular wings in parallel movement and rotation. They are therefore also suitable for judging devices which respond to differences in the pressure distribution. For example we may recall the "Betz-Schlitze,"[14] which are provided for the top of the wing and the external part of the wing halves and are used to reduce the high speed rotation in spin flight.

5. Finally it should also be mentioned that the measurement results given could contribute to the clarification of the question as to how far the proposal to study the processes on the aircraft rotating in free space with a model[15] fixed in the rotating

---

[14] See footnote 3b.

[15] M. Kramer and K. B. Krüger, . new spin measurement device, Luftf.-Forschg. Vol. 14 (1937), pp. 475-479.

experimental jet, which is important because of its advantages under the experimental technology aspect, could be successful. According to the existing results, the method will give for fixed flow attached on all sides and for all the rotation values considered practically satisfactory results which can also be applied for fully separated flow and lower values of rotation. For a flow which is undergoing transition from the attached to the separated state or for totally separated flow and higher rotational values, however, the reliability of the method may be disputed.